Cell Reports
Methods

Article

Non-invasive ovulation tracking enables genetic engineering in wild rodents

Graphical abstract

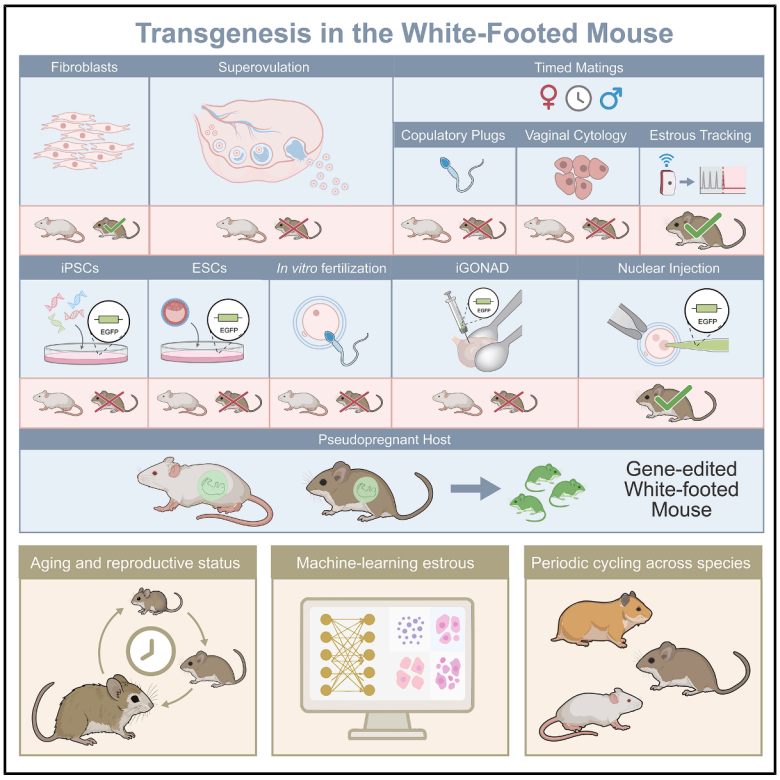

Highlights

- Methods for embryo harvesting, pseudopregnancy, and genetic engineering of *P. leucopus*
- Camera-based activity tracking enables reliable detection of ovulation in wild rodents
- Approach generalizes across species, revealing conserved estrous-linked activity
- Camera-based estrous tracking reveals a non-invasive physical biomarker of reproductive aging

Authors

Joanna Buchthal, Emma J. Chory, Zachary Hill, ..., Styliani Markoulaki, Rudolf Jaenisch, Kevin M. Esvelt

Correspondence

buchthal@mit.edu (J.B.), esvelt@mit.edu (K.M.E.)

In brief

Buchthal et al. develop a camera-based estrous-tracking method that reliably detects ovulation in wild rodents. This non-invasive approach overcomes barriers to genetic engineering in *Peromyscus leucopus*, enables transgenesis, generalizes to additional species, and identifies reproductive aging phenotypes through behavioral signatures. This work advances tools needed for disease-resistant reservoir models.

Buchthal et al., 2026, Cell Reports Methods *6*, 101311
February 23, 2026
https://doi.org/10.1016/j.crmeth.2026.101311

CellPress

Cell Reports Methods

CellPress
OPEN ACCESS

Article

Non-invasive ovulation tracking enables genetic engineering in wild rodents

Joanna Buchthal,[1,2,15,*] Emma J. Chory,[1,3,4,15] Zachary Hill,[1] Christy Dennison,[1] Boqiang Tu,[1,3] Rick P. Wierenga,[1] Çağrı Çevrim,[5] Stefan Golas,[1] Gabriel Meier,[6,7] Tammy C.T. Lan,[8,9] Hattie Chung,[10] Magalie Boucher,[11] Sam R. Telford,[12] Kara L. McKinley,[5,13] Styliani Markoulaki,[6] Rudolf Jaenisch,[6,14] and Kevin M. Esvelt[1,16,*]

[1]Media Laboratory, Massachusetts Institute of Technology, Cambridge, MA 02139, USA
[2]Mice Against Ticks, Lincoln, MA 01773, USA
[3]Department of Biological Engineering, Massachusetts Institute of Technology, Cambridge, MA 02139, USA
[4]Department of Biomedical Engineering, Duke University, Durham, NC 27705, USA
[5]Department of Stem Cell and Regenerative Biology, Harvard University, Cambridge, MA 02138, USA
[6]Whitehead Institute for Biomedical Research, Cambridge, MA 02142, USA
[7]RNA Biology and Molecular Physiology, Faculty for Biology, Bielefeld University, Bielefeld, Germany
[8]Broad Institute of Harvard and MIT, Cambridge, MA 02142, USA
[9]Department of Molecular and Cellular Biology, Harvard University, Boston, MA, USA
[10]Yale University School of Medicine, New Haven, CT 06520, USA
[11]Division of Comparative Medicine, Massachusetts Institute of Technology, Cambridge, MA 02139, USA
[12]Department of Infectious Disease and Global Health, Tufts University, Grafton, MA 01536, USA
[13]Howard Hughes Medical Institute, Cambridge, MA 02138, USA
[14]Department of Biology, Massachusetts Institute of Technology, Cambridge, MA 02139, USA
[15]These authors contributed equally
[16]Lead contact
*Correspondence: buchthal@mit.edu (J.B.), esvelt@mit.edu (K.M.E.)
https://doi.org/10.1016/j.crmeth.2026.101311

MOTIVATION The white-footed mouse is an ecologically and medically important model species—long-lived, behaviorally tractable, and a natural reservoir for tick-borne pathogens. Yet, efforts to genetically engineer *Peromyscus leucopus* have long been hindered by inefficient and ineffective reproductive protocols—challenges common to many non-model rodents. These constraints have made it nearly impossible to generate embryos or pseudopregnant recipients, effectively preventing transgenesis. Repeated failures to adapt *Mus* protocols underscore the need for accessible reproductive strategies suited to diverse species. To address this gap, we developed a non-invasive method for reliably tracking ovulation, which enabled genetic engineering in a species previously considered intractable and offers a generalizable tool for advancing non-model rodent research.

SUMMARY

Many non-model rodent species are inaccessible to genetic engineering due to our limited understanding of their reproductive biology. Here, we present a low-cost, camera-based estrous-tracking technology that enables transgenesis in the white-footed mouse *Peromyscus leucopus*, a key reservoir for Lyme disease. We demonstrate the efficient generation of pregnant and pseudopregnant mice via timed ovulation, provide protocols for embryo generation, cultivation, microinjection, and transplantation as well as an accurate developmental timeline, and report the first engineered *Peromyscus*. The same technology successfully tracked conserved estrous-linked cycling behavior in other rodents, including hamsters. Finally, estrous tracking differentiated reproductively healthy, geriatric female *Peromyscus* from those with declining fertility based solely on their activity, providing a non-invasive method for studying reproductive senescence. Collectively, these tools represent a critical resource for engineering non-model rodents, advance the long-lived *Peromyscus* as a model organism, and will prove essential to heritably immunizing wild rodent populations against Lyme disease.

INTRODUCTION

The white-footed mouse *Peromyscus leucopus* is a key reservoir in the transmission of zoonotic diseases, including Lyme disease, babesiosis,[1] anaplasmosis,[2] among others.[3] With much longer lifespans and patterns of genetic diversity more closely corresponding to humans than those of laboratory mice,[4] *Peromyscus* are promising models of human aging and the pathologic basis of diseases. Given their ecological importance and potential value to biomedical research, the ability to generate genetically engineered *Peromyscus* models would have widespread utility.

Since the first transgenic laboratory mice were engineered with viral DNA,[5] scientists have developed increasingly powerful strategies for generating new animal models. Stem cell-based transgenesis technologies, which leverage mouse embryonic stem cells (mESCs) and induced pluripotent stem cells (iPSCs),[6] and, more recently, CRISPR-Cas9 for zygote engineering,[7] constitute some of the most robust engineering approaches. Other techniques include i-GONAD, a method for delivering DNA via intraoviductal injection followed by *in vivo* electroporation,[8] as well as *ex vivo* and *in vivo* genome editing using recombinant adeno-associated viruses (rAAVs)[9] and the lentiviral vector-mediated transduction of spermatozoa via *in vitro* fertilization.[10] All were originally developed in *Mus musculus*, and some have been successfully applied to engineering other species.[11–13] However, transgenesis has yet to be achieved in *Peromyscus*, and many other non-model rodents remain resistant to such engineering efforts.

Diverging from *Mus* over 25 million years ago, *Peromyscus* exhibit a range of biological differences, from "hidden" internal copulatory plugs without cervical projections to extended gestational timelines and low-efficiency mating.[14–16] Attempts to apply conventional *Mus* reproductive protocols to *Peromyscus* have failed because researchers cannot use standard techniques like "plug checking" to verify mating and confirm pseudopregnancy. As a result, researchers have turned to vaginal lavage and cytology for estrus and mating detection. However, the *P. leucopus* estrous cycle appears highly variable by vaginal cytology, with estrous cycles lasting between 2 and 8+ days, despite an assumed estrous cycle of 4 days (mode = 4, median = 4.9, average = 6).[17] Further, the use of vaginal lavage to detect sperm appears to be minimally predictive of fertilization events, as researchers have routinely found sperm in vaginal smears from non-gravid *P. leucopus*.[14] Consequently, timed mating has been reported to be highly inefficient in *P. leucopus*, with a published pregnancy rate of 20% in females mated with males to satiety.[14] To increase pregnancy rates and embryo yields, other researchers have incorporated *in vitro* maturation of oocytes to compensate for failed follicle rupture following hormone treatment[18] or combined superovulation, timed mating, and artificial insemination, but still they have produced only a fraction of the embryos that are typically harvested by superovulation alone in *Mus*.[19] These challenges are not unique—developing reproductive protocols in non-model rodents such as hamsters and voles has also proven consistently difficult, with even low doses of gonadotropins impairing embryo quality in Syrian hamsters and significant genetic background effects limiting superovulation efficiency in prairie voles.[20,21] Since mating events in *Peromyscus* occur without giving rise to pregnancy, more recent advances such as mating detection with cameras are also unlikely to be successful.[22,23] Thus, it will not be possible to apply established forms of genetic engineering to *Peromyscus* until there are reliable reproductive protocols for generating timed pregnant females.

In this work, we detail our efforts to engineer *Peromyscus* with camera-based tools that elucidate their reproductive biology and extend their use to other non-model species. We specifically sought to engineer the long-lived *P. leucopus*, the primary reservoir of the Lyme disease pathogen *Borrelia burgdorferi*, as engineering the reservoir may lead to new ecological tools for combating Lyme disease.[24] After multiple failed attempts at transgenesis via standard techniques, we developed an accessible and broadly enabling solution for improving mating efficiency, first using implanted sensors that detect estrous-dependent changes in body temperature, and subsequently via low-cost camera-based activity tracking. With reliable estrous monitoring, we generated pregnant and pseudopregnant *Peromyscus* at rates nearing those for *Mus*, and performed targeted transgenesis with CRISPR-Cas9. We additionally applied camera-based activity tracking to monitor highly divergent species, including *Mus* and Syrian hamsters, and to gather training data for a machine learning model that predicts estrous cycle day based on vaginal cytology, offering improved *Peromyscus* cytological analysis without camera networks. Finally, we show that camera-based activity tracking can distinguish reproductively healthy, geriatric *Peromyscus* from those showing signs of reproductive aging, thereby providing a new and non-invasive tool for investigating the mechanisms that govern female reproductive health.

RESULTS

Efforts to engineer *Peromyscus* ESCs and iPSCs

Our *Peromyscus* engineering efforts began with an attempt to derive embryonic stem cells (ESCs) from blastocysts, using an optimized superovulation protocol (Figure S1A) (see supplemental information) that proved highly inefficient in our colony. Briefly, a small number of embryos were recovered at all stages of embryogenesis (Figure S1B) but embryos harvested at the 8-cell stage developed best *in vitro*. In total, we performed 5 rounds of ESC derivation (Figure S1C). Our first attempt, using mESCD-KSR medium,[25] resulted in small, round, tightly formed colonies that were bright under phase contrast but differentiated at a high rate, failed to reliably expand, and disappeared after several passages (see supplemental information). In our fifth attempt, mESCD-KSR-2i medium facilitated the growth of ESC-like colonies that successfully propagated. Pluripotency was assessed by staining for pluripotency markers (Figure S1D) and by performing a teratoma formation assay, which provided evidence of ESC contribution to the mesoderm and ectoderm (Figure S1E). However, we consistently encountered issues with ESC expansion and differentiation. As such, we simultaneously attempted to derive iPSCs from *Peromyscus* mid-gestational fetal fibroblasts that had been infected with human cDNAs for KLF4, OCT4, SOX2, and c-MYC under TetO control

(Figure S1F).[26] In the presence of doxycycline, we observed colonies with an apparent iPSC morphology, but no dox-independent clones were obtained upon withdrawal.

We next attempted CRISPR-based engineering of our ESC lines at the Rosa26 locus by first comparing our *de novo* sequenced *Peromyscus* genome with previously published Rosa26 *Mus* knock-ins (Figure S2A).[27] Following nucleofection, two EGFP$^+$ ESC cell lines were generated using two different constructs containing either CMV or CAG (Figure S2B), but only the CAG promoter produced homogeneous populations of bright EGFP$^+$ cells (Figure S2C). While ESCs remained puromycin-resistant and EGFP$^+$ after multiple passages, karyotyping revealed trisomies for chromosomes 16 and 17 (Figure S2D). Due to abnormal karyotyping and the aforementioned challenges with ESC expansion and propagation, efforts to further develop stem cell-based strategies for genetic engineering were paused.

In situ germline genome engineering via i-GONAD

We next attempted to engineer *Peromyscus* embryos with i-GONAD, an electroporation method that has been used to genetically modify multiple rodent species (Figure 1A).[8] We first validated that our intraoviductal injection and electroporation technique successfully delivered EGFP mRNAs into preimplantation embryos, which fluoresced when recovered (Figure S2E). We next used i-GONAD to deliver CRISPR RNPs, including our validated *Peromyscus* Rosa26 guide. In total, we performed 39 i-GONAD procedures, which gave rise to 4 litters, only two of which survived. Sequence analysis showed that one of the two litters contained a single gene-edited pup with a mutation in the *Peromyscus* Rosa26 locus (Figure S2F).

Although successful, i-GONAD proved to be highly inefficient in *Peromyscus*, yielding only one gene-edited pup after nearly 40 surgeries (Figure 1B). The poor efficiency may have been exacerbated by a low fertilization rate, since females were chosen for the procedure based on the presence of sperm, an unreliable pregnancy marker in *P. leucopus*.[14] Moreover, repeated handling may have triggered pregnancy block, a stress-induced failure of embryo implantation previously documented in experimentally manipulated animals.[28]

Estrous tracking with core body temperature

Over the course of the estrous cycle, the mice experienced numerous physiological changes due to hormonal fluctuations (Figure 1C).[29,30] In particular, the release of progesterone causes a corresponding rise in body temperature around the time of ovulation. As a result, core body temperature telemetry has been used to arrange highly efficient timed matings and detect early pregnancy in *Mus*.[31] We sought to apply the same telemetry system to *Peromyscus* to improve timed mating by implanting sensors (G2 E-Mitter, Starr Life Sciences, Oakmont, PA) in the abdominal cavity of 10- to 16-week-old females. These sensors track core body temperature and locomotor activity when coupled with a receiver that powers them and collects measurement data over time (Figure 1D). Temperature readings were collected once per minute during the study (Figure 1E).

In accordance with the established *Mus* estrous cycle,[32] ovulation events in *Mus* were detected with implanted temperature sensors every 4–5 days as prolonged heat periods that extend into the daily rest period.[31] Following sensor implantation, we observed similar cycling patterns in *Peromyscus* beginning 3–14 days post-surgery (Figure 1F) A 4-day estrous cycle was detected in 9 out of 11 animals, with core body temperature peaking after the lights were on (Figure S3). This trend was apparent for both individual mice and the population average (Figure 1G). In total, 57 temperature sensor implant surgeries were performed, and 36 cycling mice were identified (Figure S4). The rate of cycling across all experiments (63%) is consistent with the reported rate of cycling among *P. leucopus* in a previous study (61%) (Figure 1H).[17]

Pregnancy with estrous tracking

We next tested whether timed mating could be improved in *P. leucopus* by introducing males on the night of presumed ovulation based on core body temperature. Fifteen females with implanted sensors were monitored for estrous cycling and mated on the night of presumed ovulation (Figure 1I). After 4 days, suspended estrous cycles were observed in 14 out of the 15 mice (Figure S5A). The high rate of estrous cycle disruption was readily apparent in the population average (Figure 1J). Eleven of the 15 *Peromyscus* produced litters after 24–26 days, with an average litter size of 3.4 pups (Figure S5B). Importantly, female mice that were mated two nights prior to the night of ovulation recorded overnight temperature spikes indicative of mating activity without exhibiting signs of estrous cycle disruption (Figure 1K); periodic estrous-linked heat fluctuations continued unabated (Figure 1L). Interestingly, the telemetry system also revealed a subset of mice that experienced pregnancy-like events, with 3 mice exhibiting a break in estrous cycling that lasted for at least 20 days (Figure S5A). Overall, mouse core body temperature telemetry for timed mating had more than quadrupled the efficiency of pregnancy or pregnancy-like events in *P. leucopus*, from 20% to 93% (Figure 1M).

Estrous tracking with animal activity

As with core body temperature, researchers have observed elevated activity in *Mus* around the time of ovulation.[31] However, activity tracking was previously deemed inadequate for timed mating because ovulation events could only be detected in averaged activity data, not for individual mice.[31] As such, we initially focused our efforts on improving timed mating with core body temperature readings alone. However, once temperature-based ovulation detection was established, we observed that temperature readouts were highly correlated with concurrent activity data collected by the same sensors, which detected movement through changes in voltage across an internal capacitor (Figure S5C). Notably, we were able to clearly identify a prolonged extension of activity in individual mice on days of ovulation (Figure S5D), a trend that was similarly visible at the population level (Figure S5E).

Development of camera-based activity tracking for estrous detection

While telemetry enables efficient mating, it requires invasive surgery that disrupts the cycle for ~13 days and costs >$1,575 per sensor—too costly for broad adoption. Unlike surgically

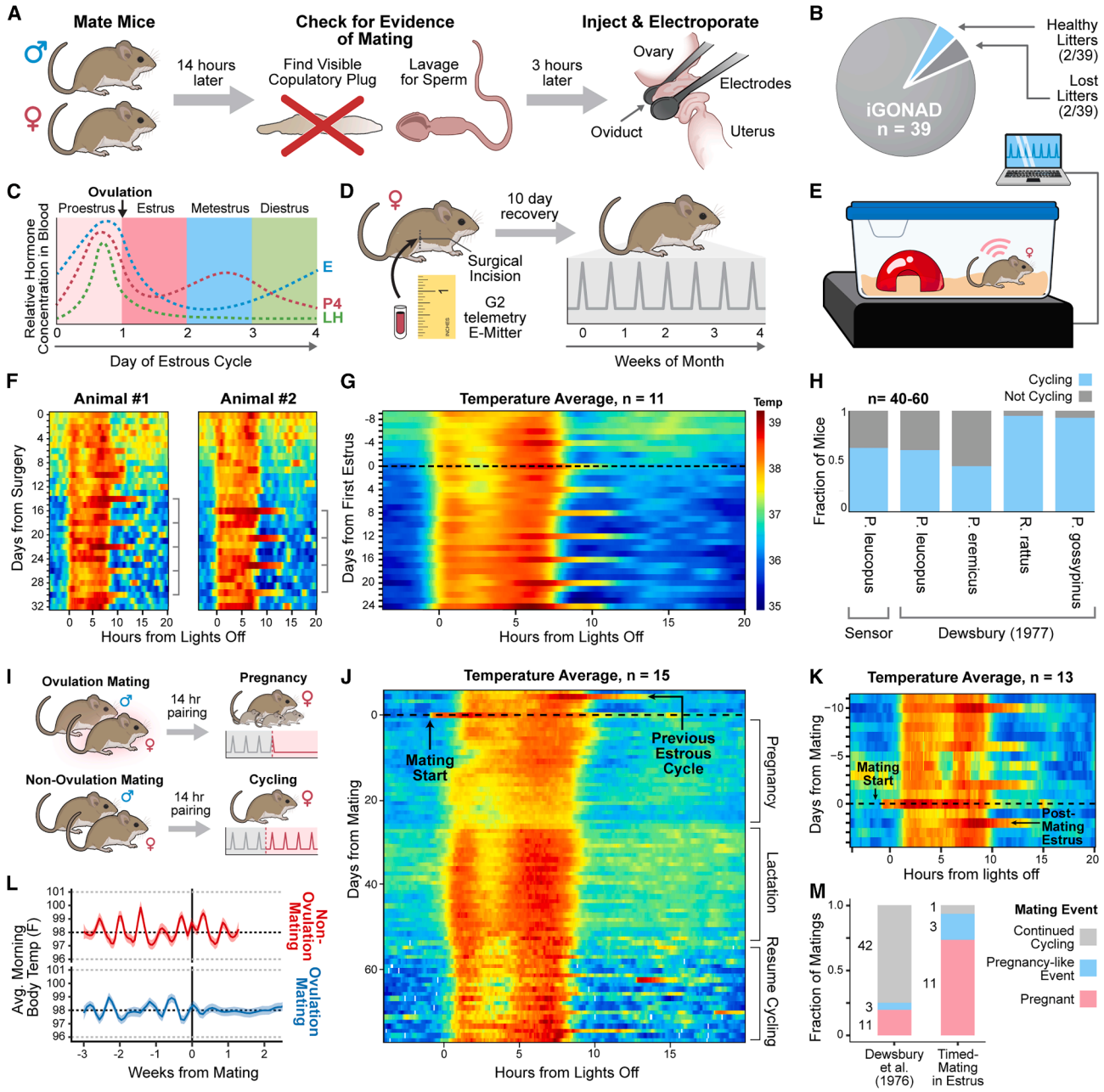

Figure 1. Core body temperature monitoring reveals the *Peromyscus* estrous cycle and enables highly efficient timed mating

(A) i-GONAD schematic.
(B) i-GONAD outcomes.
(C) *Mus* estrous cycle.
(D) Telemetry system.
(E) Data transmission.
(F) Core body temperature data from two *Peromyscus*, stacked by day; ovulation appears as prolonged peaks.
(G) Mean temperature for 11 cycling mice.
(H) Sensor-based cycling rate vs. literature.
(I) Timed mating schemes.
(J and K) Mean temperature for females mated on ovulation night (J) and two nights earlier (K).
(L) Morning temperature in pregnant vs. non-pregnant mice.
(M) Timed pregnancy efficiency: telemetry vs. lavage/cytology.

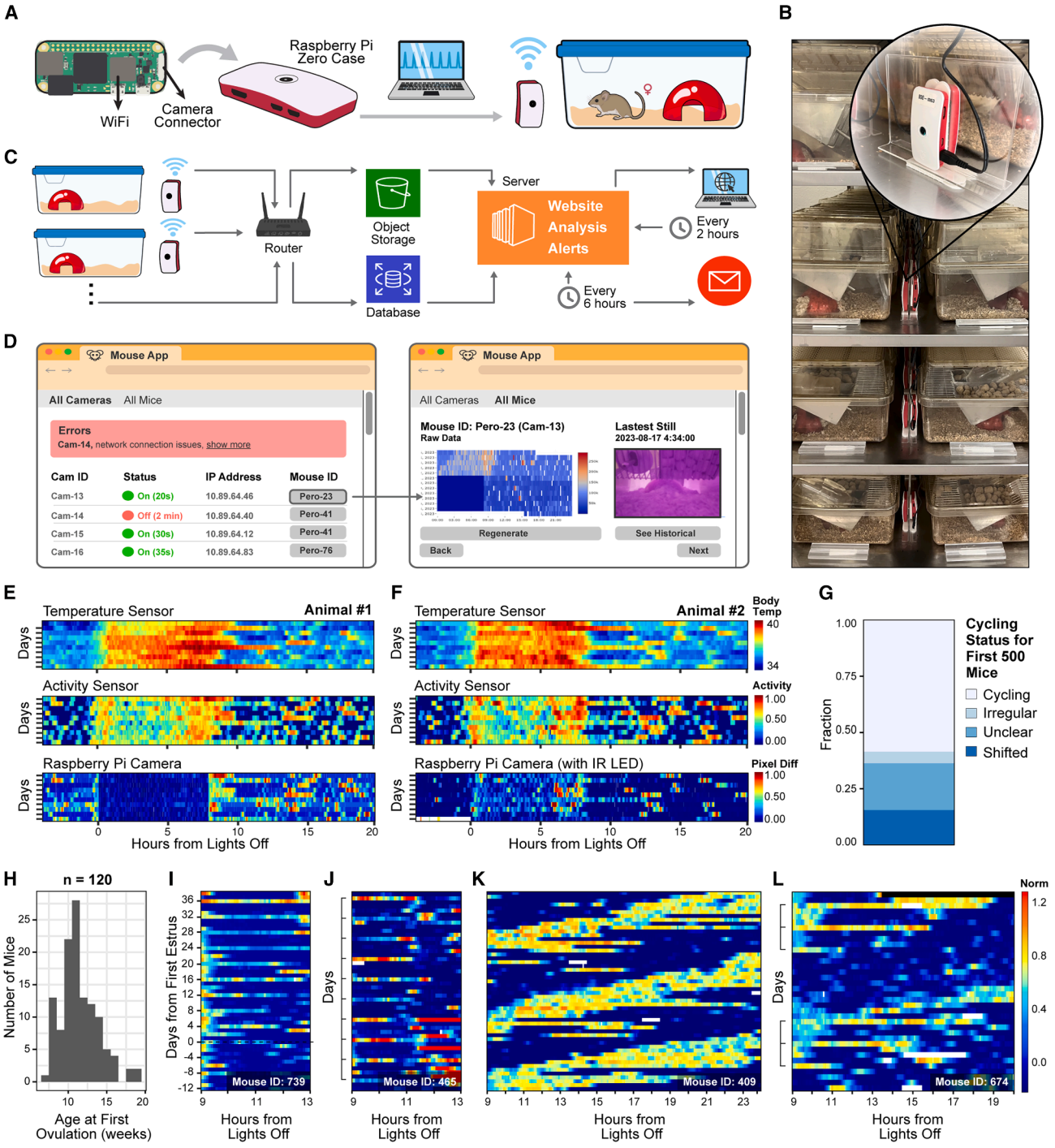

Figure 2. Camera-based activity tracking detects the estrous cycle and reveals behavioral patterns

(A) Camera system schematic.

(B) Photo of rack-mounted cameras.

(C) Data pipeline.

(D) Web interface.

(E and F) Simultaneous recordings: core temperature, sensor activity, and camera activity for two mice, with or without night-time tracking.

(G) Cycling status of 500 mice.

(legend continued on next page)

implanted sensors, camera technology is cheap, widely available, and non-invasive. We consequently developed a camera system for tracking *Peromyscus* activity using the Raspberry Pi, a low-cost single-board computer. *Peromyscus* cages were equipped with a Raspberry Pi Zero 2 W (Wi-Fi-enabled) computer attached to a Raspberry Pi NoIR V2 camera module capable of medium-resolution photographs (Figure 2A). We outfitted three mouse racks with 210 Raspberry Pi units (Figure 2B). The camera module captures images at 4-s intervals, which are then processed on the Raspberry Pi units and the resultant activity data uploaded to our cloud database. Every 2 h, these data were downloaded to the server, processed further, and cached for fast visualization. Email alerts were sent every 6 h for failed uploads (Figure 2C). We also created a web interface to view activity patterns and simplify equipment monitoring and troubleshooting (Figure 2D).

As the G2 E-Mitter can detect lateral cage movements as readily as vigorous scratching, we first sought to validate that the estrous cycling activity was detectable via camera by placing a Raspberry Pi camera adjacent to a cage with a mouse with an implanted sensor. In doing so, we were able to simultaneously track core body temperature and locomotor activity from the sensor, along with all movements detected by the camera (Figure 2E). Estrous cycling was easily identifiable by all three readouts, with ovulation days as recognizable by the Raspberry Pi as by telemetry. We further observed that the addition of a near-IR LED provided comparable resolution during the daytime while also enabling night-time tracking (Figure 2F).

Insights from camera-based activity tracking

Observations of more than 500 female mice placed under camera-based monitoring revealed that the estrous cycling rate in our colony closely matched the rate initially detected through surgical telemetry (Figure 2G). Having demonstrated the reliability of our camera-based approach, we next sought to comprehensively characterize the activity-linked behavior patterns in *Peromyscus*. Female *Peromyscus* are thought to reach sexual maturity between 46 and 51 days of age.[33] However, monitoring a cohort of prepubescent mice through sexual maturity identified a later onset of estrous behavior (mean = 11.5 weeks, SD = 2.5 weeks) and a broader spectrum of potential estrous initiation ages (Figure 2H). First estrous behavior is easily distinguished from non-estrous activity (Figure 2I) and manifests as a consistent 4-day cycle, with few exceptions—fewer than 5 of over a thousand mice exhibited 5-day cycles (Figure 2J).

Camera-based activity tracking also revealed shifted circadian rhythms in approximately 20% of camera-tracked mice (Figure 2K). Though *Peromyscus* are frequently used as behavior models, sleep pattern irregularities have not been previously documented in the literature. However, altered sleep patterns became evident soon after the mice were monitored using cameras and remained consistent; they neither developed gradually nor dissipated over time. In some cases, estrous cycling could still be observed among the mice with shifted circadian rhythms (Figure 2L).

Timed mating for embryo production

As previously mentioned, our initial superovulation protocol proved highly inefficient, consistently yielding no more oocytes than can be recovered by harvesting on estrus without hormone stimulation (Figures 3A and S6A). In subsequent experiments that included mating, the average yield per mouse remained below five embryos and displayed marked inconsistency, with one experiment yielding fewer than one embryo per mouse (Figures 3B and S6B). To identify the source of variability, we tracked the number of cells harvested from individual mice. We quickly discovered that a small group of mice were producing the vast majority of eggs (Figure 3C), leading to experimental inconsistency. Additionally, our fertilization rate was far lower than anticipated—eggs harvested after superovulation and mating were seldom fertilized (Figure 3D). Following the identification of a clear 4-day estrous cycle, we implemented the standard *Mus* superovulation regimen of 48 h between hormone doses, only to observe equally low rates of fertilization (Figure 3D). We next compared timed mating and superovulation for embryo generation efficiency, as researchers previously demonstrated that *Mus* oocytes and the embryos produced by natural mating are often of higher quality than those produced after administering exogenous gonadotropins.[34,35] The mice were tracked via camera and mated on the night of presumed ovulation, and embryos were harvested. This approach yielded far more uniform results; the variation in cells per animal decreased substantially (Figure 3E), while the number of fertilized embryos per mouse surged (natural mating mode embryos per mouse = 5, superovulation mode embryos per mouse = 0). Timed mating was also more efficient; female mice consistently generated eggs, and the majority were fertilized (Figure 3F). Younger mice produced fewer unfertilized eggs (Figures 3G and S6C). Attempts to align superovulation with the estrous stage resulted in yields lower than those achieved through natural mating (Figure S6D).

Pseudopregnancy with estrous tracking

Most transgenesis protocols require pseudopregnant recipient females to be identified by copulatory plugs, which are not readily observable in *P. leucopus*.[16] We consequently sought to use estrous tracking to generate pseudopregnant *Peromyscus*. Six female *Peromyscus* with implanted temperature sensors were mated with vasectomized males on the night of presumed ovulation (Figure 4A). After 4 days, suspended estrous cycles were observed in 5 of the 6 mice. The high rate of estrous cycle disruption was apparent among the population average, as the early morning temperature pattern shifted from regular, cycle-linked increases to irregular or flattened profiles (Figure 4B). All mice resumed cycling roughly 2 weeks later (range = 10–14 days) (Figure S4). When core body temperatures are compared, pseudopregnancy closely resembles

(H) Age at estrous onset.
(I) Example of estrous onset.
(J) Example 5-day cycle.
(K and L) Mice with shifted circadian rhythms, with or without detectable estrous cycling.

CellPress
OPEN ACCESS

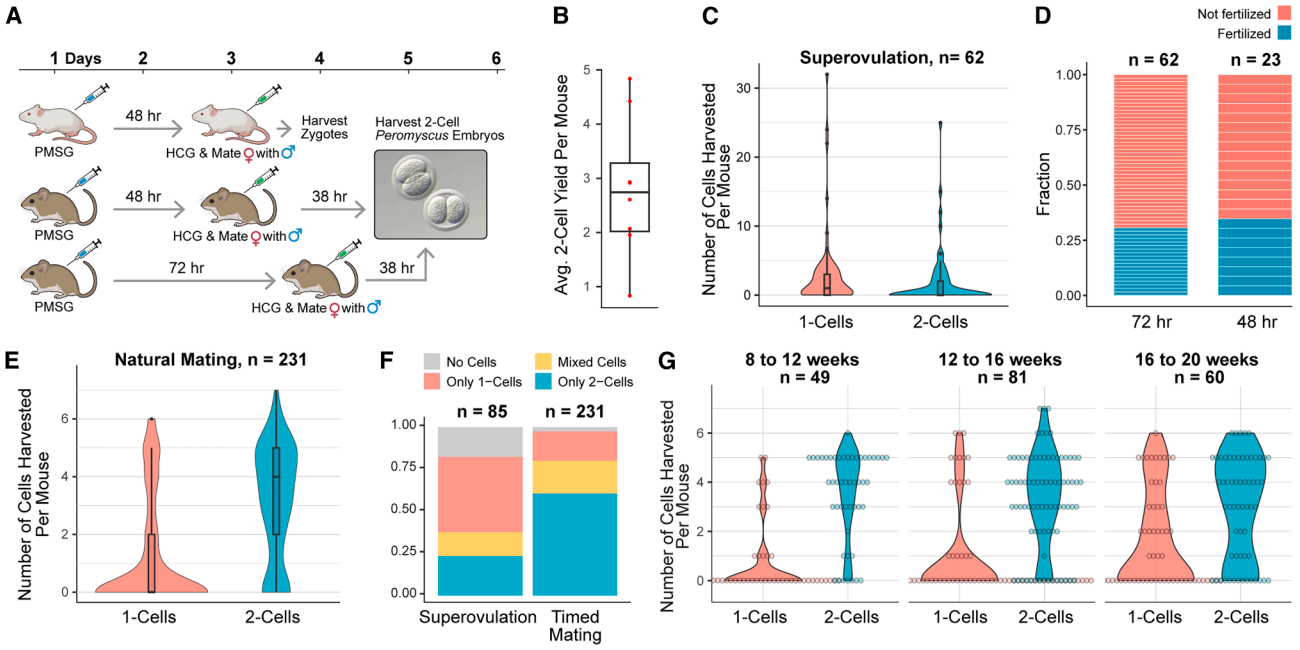

Figure 3. Timed mating via camera tracking improves embryo yield and reduces variability

(A) *Mus* vs. *Peromyscus* superovulation protocols.

(B and C) Embryo yields following 72-h PMSG-HCG protocol, pooled (B) and per mouse (C).

(D) Fertilization rates: 72-h regimen vs. 48-h regimen.

(E) Embryo yield per mouse after natural mating.

(F) Cell type distributions: superovulation vs. timed mating.

(G) Embryo yield by age following timed mating.

pregnancy in *Peromyscus*, differing only in duration, as the suspension of the estrous cycle is shorter during pseudopregnancy (Figure S7A). Next, a total of 53 camera-tracked *Peromyscus* were mated with vasectomized males and observed for cycle disruption; 85% (45/53) exhibited suspended estrous (Figure 4C). Interestingly, of the 8 mice with continued cycling, 6 had their cycles shifted by day 1 post-mating (Figure S7B).

P. leucopus developmental timelines *in vivo* and *in vitro*

Though the later stages of the developmental timeline for *P. maniculatus* are well-documented,[36] the underlying gestation data remain variable due to the lack of reliable timed mating. There is also scarce information on early *Peromyscus* development. We consequently sought to establish a comprehensive developmental timeline for *P. leucopus*, which can help determine the optimal timings for embryo harvest and transfer. We performed 40 timed matings with the camera-tracked mice and recovered embryos for every early gestational time point, daily and throughput development (Figure 4D). For the early gestational stages, we mapped the cell types retrieved at each time point (Figure 4E). Pronuclei became visible at 13 h post-mating (or after 18 h in total, assuming fertilization occurs at the midpoint of the dark cycle), whereas the *Mus* pronucleus appeared 5–11 h after fertilization. Compared with *Mus* embryos, *Peromyscus* embryos exhibited extended 2-cell stages, persisting until E2.5, and demonstrated delayed blastocyst development, with blastocysts forming on day E5.5 (Figure 4F). Blastocyst implantation appeared to occur on or before E6.5, as no cells were recovered at this time point. Since transgenesis protocols often involve overnight embryo culture, we next sought to evaluate *in vitro* embryo development. Briefly, harvested 2-cell embryos from timed mated mice were cultured in KSOM medium and housed in a tri-gas incubator until blastocysts formed. Embryos were imaged daily in order to construct an *in vitro* developmental timeline (Figure 4G). Given the low rate of development to the blastocyst stage (44%) and a 24-h delay in development with blastocysts appearing on day E6.5, we chose to forgo overnight culture and instead proceeded by harvesting at the 2-cell stage.

P. leucopus embryo transfer and nuclear injection in 2-cell stage embryos

In preparation for embryo transfer, we sought to determine the ideal number of transplanted embryos based on the natural capacity of *Peromyscus* oviducts. We accordingly harvested embryos from 202 time-mated mice and recorded the number from each uterine horn (Figure 4H). Noting a maximum of 5 embryos per horn, we hypothesized that transferring 4 embryos would have the greatest potential for successful implantation. We began by transferring unedited embryos to establish the baseline efficiency without nuclear injection. Four 2-cell embryos were transferred into 12 recipients, and 6 recipients produced a total of 15 pups or mid-gestation fetuses, with the embryo transfer efficiency improving over time (from 2/6 recipients to 4/6

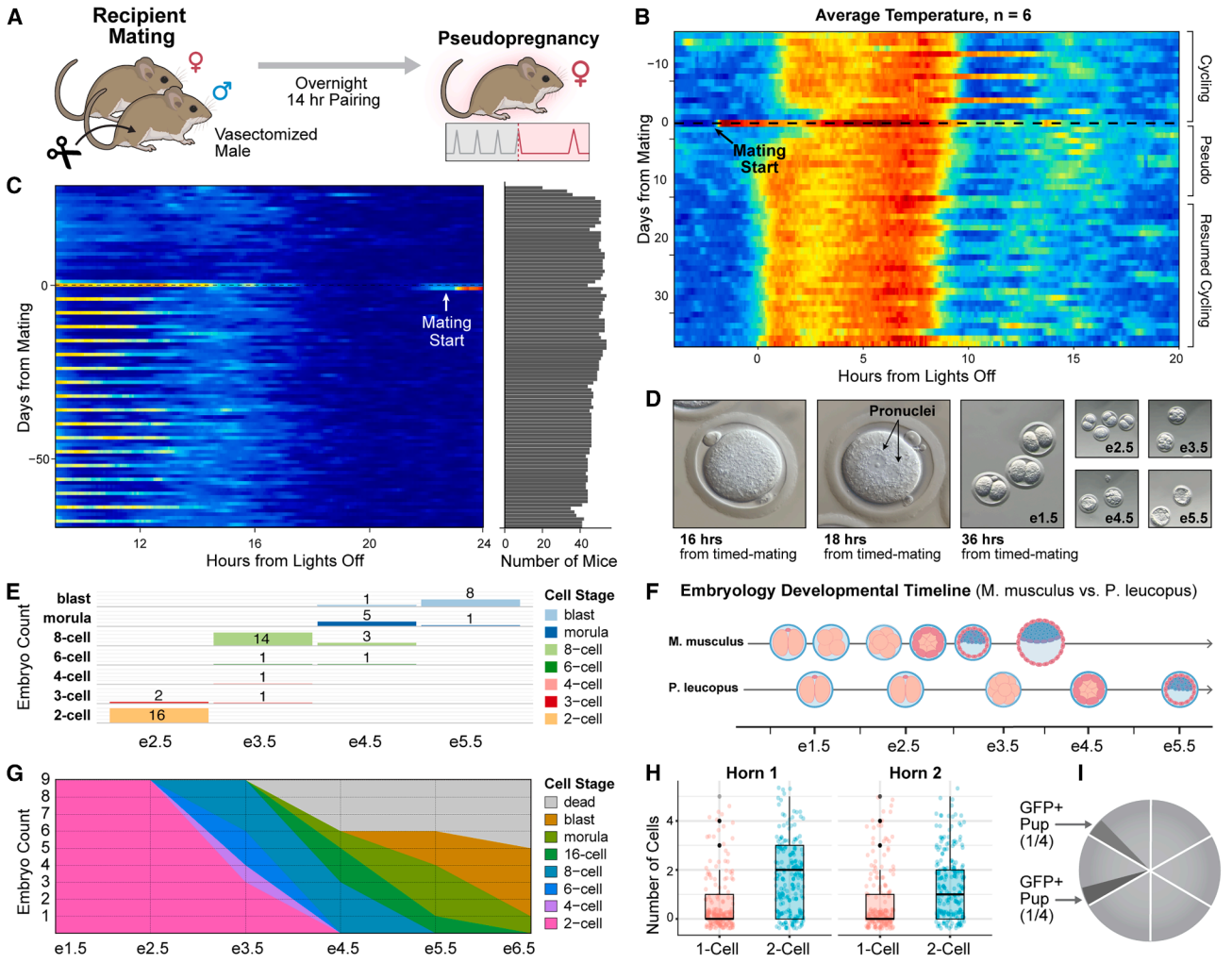

Figure 4. Camera tracking enables pseudopregnancy, developmental timelines, and genome engineering

(A) Pseudopregnancy mating scheme.

(B) Mean temperature of 6 females after mating with vasectomized males.

(C) Activity plots of 53 females post-mating with vasectomized males.

(D) Images of early embryonic stages.

(E) Cell types harvested during E2.5–E5.5.

(F) Gestational timelines for *Mus* and *Peromyscus*.

(G) *In vitro* development of 2-cell embryos.

(H) Embryo numbers per uterine horn.

(I) Genome editing outcomes: two GFP^{+} pups from six recipients, each receiving four engineered embryos.

recipients). We next sought to demonstrate genome engineering by performing nuclear injection with CRISPR-Cas9, using our previous targeting construct with the selection marker removed (Figure S2B). A total of 24 CRISPR-injected, 2-cell embryos were transferred into 6 recipients (four per mouse). Two pups were delivered, both of which were GFP-positive, resulting in an 8% conversion rate with 100% of delivered pups containing the insert (Figures 4I and S8).

Camera-based activity tracking of other rodent species

Researchers have long tracked rodent behavior using tools such as running wheels and motion sensors.[31,37–41] We next sought to determine whether modern cameras and image processing techniques could identify periodic, cycling activity in other rodent species. Our camera system was used to monitor female C57BL/6 *Mus musculus*, where estrous-linked activity is reportedly undetectable at the individual level,[31] and Syrian hamsters *Mesocricetus auratus*, a species that has previously exhibited estrous-associated activity, using motion detectors that only sense IR beam interruptions, lacking the capability for continuous visual tracking (Figure 5A).[42] Since *Mus* and hamsters are known to have night time cycling behaviors,[31,42] the females were tracked with IR cameras illuminated with IR light strips (λ = 940 nm).[31,42]

CellPress
OPEN ACCESS

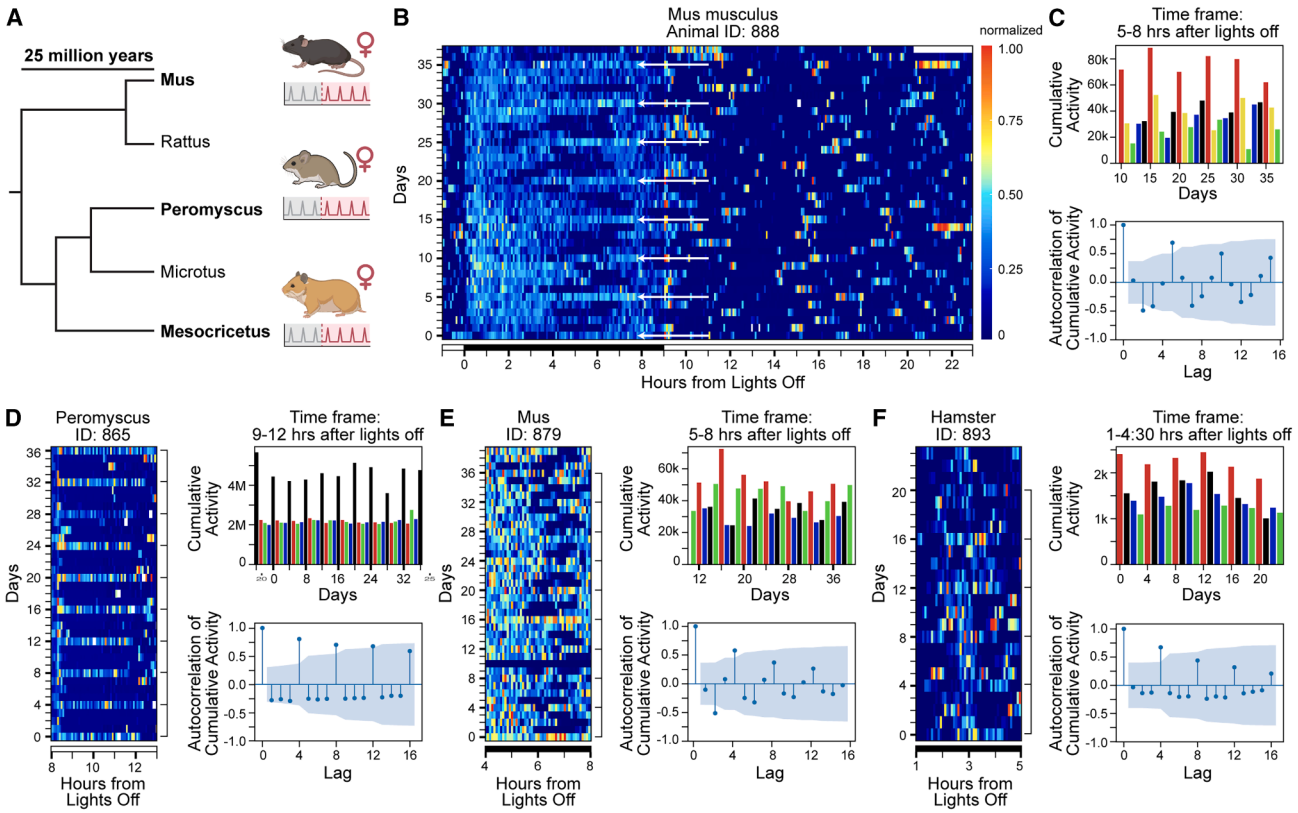

Figure 5. IR and thermal camera tracking detects periodic behavior in *Mus* and hamsters

(A) Phylogenetic tree (adapted from Bedford and Hoekstra[15]).

(B) *Mus* activity heatmap; arrows indicate cycling.

(C) *Mus* daily cumulative activity and autocorrelation plots confirm periodicity.

(D) *Peromyscus* activity heatmap, cumulative activity, and autocorrelation.

(E) Another *Mus* example with heatmap, cumulative activity, and autocorrelation.

(F) Thermal-camera hamster heatmap, cumulative activity, and autocorrelation reveal a 4-day cycle.

Shortly after the animals were placed on camera, one *Mus* was observed with a clear 5-day cycling pattern between the hours of 6:00 and 9:00 UTC (Figure 5B). However, these periodic activity trends were more difficult to discern by eye from the raw activity data. Indeed, IR illumination impeded nocturnal activity detection, as some animals became indistinguishable from the background (Figure S9A) and confounding artifacts such as reflections, shifting bedding, flickering IR light and intrinsic sensor noise were misinterpreted as movement. To better distinguish animal activity, we performed background subtraction to images by using the "TwoPoint" model (see supplemental information) and exclusively analyzed the image quadrant containing the animals' food hamper. Following image processing, *Mus* with visible cyclical behavior showed periodic cumulative activity 5–8 h after the lights were off; autocorrelation confirmed the significance of this observed 5-day trend (Figure 5C). By comparison, *Peromyscus* exhibiting clear periodic behavior (9–12 h after the lights were off) displayed much lower variability in daily cumulative activity and consequently longer periods of statistically significant autocorrelation (see lags 4, 8, and 12) (Figure 5D). Following image processing, additional *Mus* showed periodic 4- or 5-day patterns 5–8 h after lights were off. Though periodicity was not visually obvious in the activity heat maps, subtle trends emerged in some of the cumulative activity plots and were confirmed by autocorrelation as statistically significant signals (Figures 5E and S9B). Interestingly, one *Mus* displayed a shift in its cycling day over time, a behavioral change rarely seen in *Peromyscus* without mating (Figure S9C).

Following image processing (see supplemental information), additional hamsters showed cyclic behavior in cumulative activity plots, with autocorrelation confirming statistically significant periodicity (Figure S9B). To further improve activity tracking, near-IR cameras were substituted with thermal cameras, which clearly distinguished mammalian heat signatures. Subsequently, hamster activity trends became somewhat more visually apparent by activity graph 1–4.5 h after the lights were off, but statistical analysis remained essential for confirming periodicity. Although moving cage elements occasionally interfered with the signal, autocorrelation confirmed a clear 4-day cycle pattern (Figure 5F).

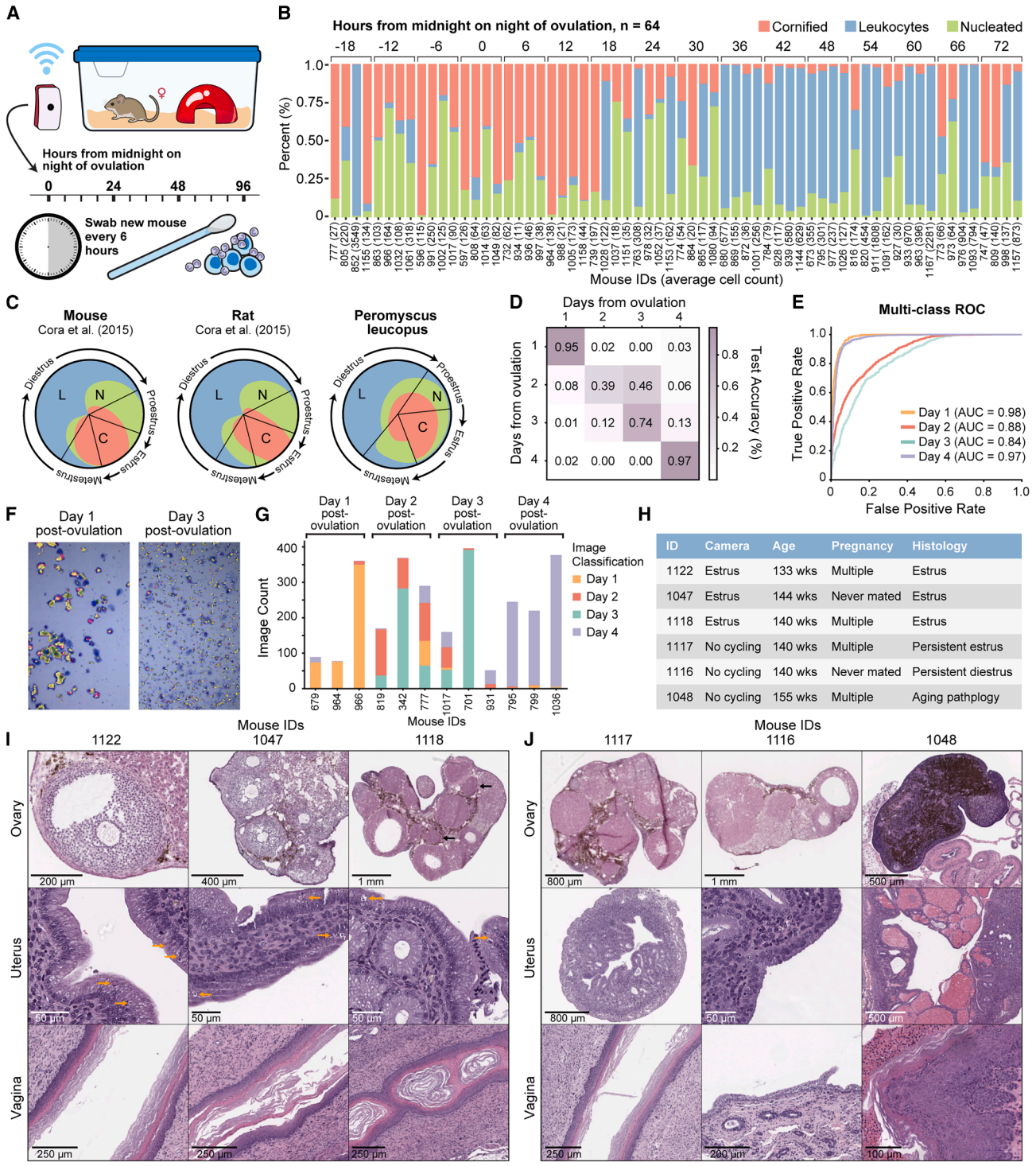

ID	Camera	Age	Pregnancy	Histology
1122	Estrus	133 wks	Multiple	Estrus
1047	Estrus	144 wks	Never mated	Estrus
1118	Estrus	140 wks	Multiple	Estrus
1117	No cycling	140 wks	Multiple	Persistent estrus
1116	No cycling	140 wks	Never mated	Persistent diestrus
1048	No cycling	155 wks	Multiple	Aging pathplogy

Figure 6. Camera tracking enhances cytology and identifies reproductive aging

(A) Swabbing timeline.

(B) Vaginal cytology plotted by hours post-ovulation.

(C) Cell type distributions across cycle stages in *Mus*, rats, and *Peromyscus* (adapted from Cora et al.[44]).

(D and E) Model confusion matrix (D) and ROC curves (E) computed using test images.

(legend continued on next page)

Improved *Peromyscus* vaginal cytology using activity tracking and machine learning

Estrous staging is essential for studying reproductive biology at a cellular level, but high variability in *Peromyscus* vaginal cytology has hindered accurate staging. We hypothesized that camera-tracked ovulation could serve as ground truth to improve cytology, providing a useful tool for labs without imaging setups. Briefly, vaginal samples were collected from groups of four *Peromyscus* every 6 h for 4 days, with a total of 64 mice swabbed (Figure 6A). Samples were imaged, and cell types were counted and plotted according to their collection time relative to ovulation (Figure 6B). Clear patterns emerged, including a long period predominated by leukocytes, in contrast to prior reports of a relatively short leukocyte-dominant period and long estrus.[43] Indeed, *P. leucopus* vaginal cytology appeared to resemble *Mus* or rat cytology (Figure 6C).[44]

To improve the accuracy of vaginal cytology readouts, we trained machine learning models to distinguish the 4 days of the *P. leucopus* estrous cycle, using cytological samples from camera-tracked mice. Briefly, 120 camera-tracked mice, across all stages of estrous were swabbed one time at 9 a.m., and the samples were imaged. The mice with high-quality images were randomly assigned to the training and validation datasets (with an 80/20 split). Five separate models were trained using the ResNet-50 architecture, which has been previously used for the automated classification of *Mus* and rat cytology.[45] Next, ensemble learning techniques were used to integrate the outputs of all five models, thereby enhancing the overall accuracy and robustness of the predictions. We tested the combined model on images from 12 unseen mice, not used for training or validation. The model demonstrated high classification accuracy for the first and last days after ovulation, moderate accuracy for the third day, and poor accuracy on the second day (Figure 6D), providing corresponding multi-class ROC curves (Figure 6E). To determine why the model was underperforming on days 2 and 3, we manually annotated cytology data from the 9 a.m. time point across all 4 days of the estrous cycle (Figure S10A). Although the cytology readouts for days 1 and 4 were distinct, day 2 readout appeared indistinguishable from day 3 readout. We next studied how the model classified images by overlaying gradient-weighted class activation maps to visualize parts of the images that were most important for the model's decisions (Figure 6F).[46] Highlighted features are primarily cells indicating the model aligns with our cytology findings. While the model associated 75% of mice with the correct estrous day, classification was more complex at the individual image level (Figure 6G). Few images were required for classification accuracy on days 1 and 4; however, accuracy was overall low on the other two days and did not improve with additional images.

With the model, a researcher using vaginal cytology requires no more than two days of swabbing. If a high confidence day is identified initially (e.g., day 1 or 4), then mice can be staged with a single swab; if a low confidence day is initially predicted (e.g., day 2 or 3), one more swab is required 48 h later for staging.

Camera-based activity tracking for monitoring female reproductive aging

Due to their long lifespans, *Peromyscus* is an emerging model organism for aging research.[47,48] We monitored a small cohort of geriatric mice, aged 24 to 36 months at the twilight of their reproductive lifespans to determine whether camera-tracking could yield insights into the biology of reproductive senescence. Three aged females with and without regular estrous cycles were identified via camera-based activity tracking (Figure S10B) and selected for necropsy to examine differences in their reproductive tracts (Figure 6H). The three cycling mice, examined on their anticipated estrus day, exhibited typical estrus histology for fertile female rats and mice with large ovarian antral F2 follicles and basophilic new corpus lutea. Uteruses featured a tall columnar surface epithelium with apoptotic epithelial cells and luminal dilation; vaginas showed a shedding cornified layer, with sloughed cells and debris in the lumen (Figure 6I) (refer to STAR Methods for histological analysis).[49–51] In contrast, all of the non-cycling mice displayed distinct phenotypes indicative of reproductive aging. One mouse exhibited characteristics of persistent estrus, including tall columnar hyperplastic endometrial epithelium and vaginal epithelium cornification—traits linked to persistent estrus in *Mus* and rats.[49,50] Another *Peromyscus* presented signs of persistent diestrus, characterized by low, cuboidal, inactive endometrial epithelium and low, somewhat mucified vaginal epithelium, as seen in rats[50]; the final mouse showed signs that it was nearing anestrus, with an atrophic ovary and cystic endometrial hyperplasia (CEH)—a condition described in aging rodents, which dysregulates the estrous cycle—and additional evidence of hormonal dysregulation/persistent estrus in the vagina (Figure 6J) (refer to STAR Methods for histological analysis).[49,50]

DISCUSSION

Peromyscus have been proposed as an improved model organism for human disease because they appear to more closely resemble humans than laboratory mice, as evidenced by hematological measurements, methylation profiles, disease susceptibility, genetic diversity, and the lifespan, which exceeds *Mus* in captivity by about 3-fold.[4,52,53] However, the dearth of genomic tools and technologies available for this species has precluded many types of research.[4] As evidenced by the many issues we encountered when propagating and expanding ESCs, generating self-sustaining iPSCs, culturing *Peromyscus* embryos, hormone priming mice, and even simply maintaining a large enough colony to support experiments without financial strain, the challenges associated with this species are formidable, and much work remains to be done.

(F) Class activation maps from trained model.
(G) Image classifications by ovulation day.
(H) Selected mice for necropsy.
(I and J) H&E-stained ovary, uterus, and vagina from cycling (I) and non-cycling (J) mice, showing features of reproductive aging.

Nevertheless, we believe our findings mark the arrival of *Peromyscus* as a tractable model organism. We present highly optimized reproductive protocols for the generation of timed pregnant and pseudopregnant *Peromyscus*. Our estrous-tracking technology is well suited for large-scale transgenesis efforts, as it is substantially more cost-effective than sensors, infrared-based systems, or running wheels, which can alter activity patterns and obscure ovulation-related behaviors.[54,55] Further, this non-invasive approach also avoids behavioral disruptions that can interfere with maternal care.[56] Unlike our camera-based approach, infrared-based systems have positional limitations that can hinder movement detection when animals remain in localized areas.[40] Effective deployment often requires cage modifications, which can introduce escape risks or create hardware vulnerabilities. Additionally, some systems rely on batteries and local data storage, necessitating frequent maintenance and manual data retrieval.[40] In contrast, our system uses continuous power and Wi-Fi connectivity to enable uninterrupted, scalable data collection with minimal intervention. When paired with image processing and quantitative analysis, camera-based tracking detected periodic activity in the laboratory mice and hamsters, even when behavioral signals were subtle, suggesting broader potential for identifying periodic behavior across diverse rodent species. Finally, we demonstrate efficient *Peromyscus* genome engineering via nuclear injection of CRISPR-Cas9, paving the way for the development of *Peromyscus* and other rodents as model organisms. Example species with translational potential include, but are not limited to, refractory species of rats, prairie voles, guinea pigs, and naked mole rats, which may help illuminate the underlying mechanisms that influence longevity,[57,58] neurogenesis,[59] social behavior patterns,[60] degeneration,[61] and susceptibility to diseases.[62]

The potential of camera-based activity tracking for biomedical research is underscored by our finding that geriatric female *Peromyscus* exhibit distinct activity patterns that correlate with reproductive health. Histological evaluation confirmed aging etiologies among non-cycling elderly mice that otherwise appeared physically identical to their cycling counterparts, suggesting it may be possible to identify new behavioral biomarkers of ovarian dysfunction and improve predictions of reproductive lifespan. Combined with transgenesis and techniques such as scRNAseq, spatial transcriptomics, and proteomics, camera tracking could facilitate longitudinal studies to explore age-related changes in gene expression, protein function, and cellular metabolism.

P. leucopus are the primary reservoir of *B. burgdorferi*, the causative agent of Lyme disease across much of North America.[1] The Mice Against Ticks project is a community-guided effort to engineer Lyme-resistant *Peromyscus* in order to disrupt the ecological transmission cycle between white-footed mice and ticks and reduce disease prevalence in hard-hit areas such as the islands of Nantucket and Martha's Vineyard[24] and potentially mainland communities using forms of gene drive.[63,64] Camera-enabled transgenesis has opened the door to engineering *P. leucopus* that heritably express anti-Lyme antibodies derived from locally sourced mice,[65] providing a new model for future rodent engineering efforts aiming to prevent zoonoses ranging from Lassa fever to hantavirus pulmonary syndrome.

Limitations of the study

This study has several limitations. First, although our reproductive protocols enabled successful engineering of *P. leucopus*, the number of donor animals required for transgenesis remains high. For example, generating 24 embryos for our GFP experiment required eight donors, a number that could be dramatically reduced with an effective superovulation protocol. Because this inefficiency may be due to continued use of the eCG-hCG regimen, anti-inhibin strategies, such as injection with anti-inhibin serum (AIS), which have proven effective in other rodent species should be systematically evaluated.[66–68] Second, while we demonstrated the utility of activity tracking across several rodent species, additional validation is needed to confirm detection of the ovulation day, particularly in species where peak activity may precede ovulation. Third, while the machine learning model improves vaginal cytology, it was trained exclusively on high-quality swabs from cycling animals and may perform less reliably in animals with disrupted or atypical cycles. Additionally, we observed low-level estrous cycle disruption (e.g., skipping or pseudopregnancy) in 4% of swabbed mice, and this effect may compound with repeated sampling. Finally, while camera-based activity tracking provided non-invasive insights into reproductive senescence, histological validation was limited to a small cohort and may not have captured the full spectrum of age-related reproductive decline.

RESOURCE AVAILABILITY

Lead contact

Further information and requests for resources should be directed to the lead contact, Dr. Kevin M. Esvelt (esvelt@mit.edu).

Materials availability

This study did not generate any unique reagents.

Data and code availability

- All source data are publicly available on Mendeley. See Mendeley Data: https://data.mendeley.com/datasets/4dn3w5b5yc/1 https://doi.org/10.17632/4dn3w5b5yc.1.
- The *Peromyscus leucopus* genome assembly has been deposited in GenBank (GenBank: JBSIEY000000000).
- Nanopore sequencing reads used for genotyping have been deposited in the NCBI Sequence Read Archive (SRA) and are available under BioProject: PRJNA1364316.
- All code is publicly available on GitHub at https://github.com/Buchthal/Peromyscus_Transgenesis/tree/main. An archival version of the codes is available via Zenodo (https://doi.org/10.5281/zenodo.17622641) and is listed in the key resources table.
- Any additional information needed to re-analyze the data reported in this study is available from the lead contact upon request.

ACKNOWLEDGMENTS

This work was supported by the Tick-Borne Disease Research Program (DoD CDMRP Award #TB160101 W81XWH-17-1-0669), the National Institutes of Health (R01 AI152209), the National Science Foundation (CAREER Award #1943141), the Rainwater Charitable Foundation, The Michael R. Paine Conservation Trust, and Mice Against Ticks, Inc. Additional support came from Esvelt lab sources, including the MIT Media Lab, an Alfred P. Sloan Research Fellowship, Open Philanthropy Project, the Aphorism Foundation, and the National Institute of Digestive and Kidney Diseases (R00 DK102669-01). J.B. was supported by the MIT Media Lab, and E.J.C. was partially supported by a Ruth L. Kirschstein NRSA fellowship from the National Cancer Institute (F32

CA247274-01). We thank Dr. Siniša Hrvatin for generously lending telemetry equipment that enabled our pilot studies. We are grateful to MIT's Division of Comparative Medicine, especially Dr. Kelly Metcalf Pate, as well as our animal care team (including Dr. Susan Erdman, Dr. Bernard Varian, Andrea Vargas, and Harlin Lemus) and pathology team (Caroline Atkinson, Ariah Lacey, and Samantha Moore) for their support. We thank the communities of Nantucket and Martha's Vineyard for their continued input and thoughtful feedback, including Dr. Roberto Santamaria, Dr. Malcolm MacNab, Dr. Emily Goldstein Murphy, Dr. Carrie Fyler, and the late Dr. Michael Loberg. We offer special thanks to Todd Rainwater, Dr. Amy Rommel, and the Mice Against Ticks board—Ana Martinez and Beth Colt—for their encouragement and guidance. We also thank Dr. Heidi Fisher for sharing her lab's superovulation protocol. This manuscript is dedicated to late Dr. Howard Dickler, whose invaluable guidance, unwavering support, and exceptional warmth are deeply missed.

AUTHOR CONTRIBUTIONS

J.B., conceptualization, formal analysis, resources, writing – original draft, visualization, project administration, and funding acquisition; E.J.C., conceptualization, formal analysis, data curation, writing – original draft, visualization, and supervision; S.R.T., resources; R.J., supervision; S.M., supervision; K.M.E., conceptualization, methodology, supervision, and funding acquisition. All authors assisted in reviewing and editing the final draft of the manuscript. Stem cell derivation/i-GONAD: J.B., conceptualization, formal analysis, and funding acquisition; Z.H., methodology and investigation (ESCs, iPSCs, and i-GONAD); G.M., investigation (i-GONAD); S.R.T., resources; R.J., conceptualization and supervision; S.M., conceptualization, methodology, and investigation (ESCs, iPSCs, and i-GONAD); K.M.E., conceptualization, methodology, resources, and funding acquisition. Temperature/camera-based estrous tracking studies: J.B., conceptualization, methodology, validation, formal analysis, investigation, and funding acquisition; E.J.C., conceptualization, methodology, software, formal analysis, and data curation; Z.H., methodology, validation, and investigation (embryo transfer and nuclear injection); C.D., methodology, software, investigation, and data curation (camera tracking); B.T., software, formal analysis, investigation, and data curation (camera tracking and cytology); R.P.W., software, formal analysis, investigation, and data curation (camera tracking and cytology); C.C., investigation (camera tracking); S.G., methodology and validation (camera tracking); T.C.T.L., methodology, formal analysis, and investigation (histology); H.C., methodology, formal analysis, and investigation (histology); M.B., methodology, investigation, and formal analysis (histology); S.R.T., resources; K.L.M., methodology and resources (camera tracking); K.M.E., conceptualization and methodology.

DECLARATION OF INTERESTS

J.B., E.J.C., C.D., and K.M.E. are inventors on a PCT application filed with the USPTO on the method. Additionally, J.B. serves as a director of the Mice Against Ticks (non-profit), and E.J.C. serves as a consultant.

STAR★METHODS

Detailed methods are provided in the online version of this paper and include the following:

SUPPLEMENTAL INFORMATION

Supplemental information can be found online at https://doi.org/10.1016/j.crmeth.2026.101311.

Received: February 11, 2025
Revised: June 17, 2025
Accepted: January 9, 2026
Published: February 17, 2026

REFERENCES

1. Spielman, A., Etkind, P., Piesman, J., Ruebush, T.K., 2nd, Juranek, D.D., and Jacobs, M.S. (1981). Reservoir hosts of human babesiosis on Nantucket Island. Am. J. Trop. Med. Hyg. *30*, 560–565. https://doi.org/10.4269/ajtmh.1981.30.560.
2. Telford, S.R., 3rd, Dawson, J.E., Katavolos, P., Warner, C.K., Kolbert, C.P., and Persing, D.H. (1996). Perpetuation of the agent of human granulocytic ehrlichiosis in a deer tick-rodent cycle. Proc. Natl. Acad. Sci. USA *93*, 6209–6214. https://doi.org/10.1073/pnas.93.12.6209.
3. Barbour, A.G. (2017). Infection resistance and tolerance in Peromyscus spp., natural reservoirs of microbes that are virulent for humans. Semin. Cell Dev. Biol. *61*, 115–122. https://doi.org/10.1016/j.semcdb.2016.07.002.
4. Havighorst, A., Crossland, J., and Kiaris, H. (2017). Peromyscus as a model of human disease. Semin. Cell Dev. Biol. *61*, 150–155. https://doi.org/10.1016/j.semcdb.2016.06.020.
5. Jaenisch, R., and Mintz, B. (1974). Simian virus 40 DNA sequences in DNA of healthy adult mice derived from preimplantation blastocysts injected with viral DNA. Proc. Natl. Acad. Sci. USA *71*, 1250–1254. https://doi.org/10.1073/pnas.71.4.1250.
6. Okita, K., Ichisaka, T., and Yamanaka, S. (2007). Generation of germline-competent induced pluripotent stem cells. Nature *448*, 313–317. https://doi.org/10.1038/nature05934.
7. Wu, Y., Liang, D., Wang, Y., Bai, M., Tang, W., Bao, S., Yan, Z., Li, D., and Li, J. (2013). Correction of a genetic disease in mouse via use of CRISPR-Cas9. Cell Stem Cell *13*, 659–662. https://doi.org/10.1016/j.stem.2013.10.016.
8. Ohtsuka, M., Sato, M., Miura, H., Takabayashi, S., Matsuyama, M., Koyano, T., Arifin, N., Nakamura, S., Wada, K., and Gurumurthy, C.B.

(2018). i-GONAD: a robust method for in situ germline genome engineering using CRISPR nucleases. Genome Biol. *19*, 25. https://doi.org/10.1186/s13059-018-1400-x.

9. Yoon, Y., Wang, D., Tai, P.W.L., Riley, J., Gao, G., and Rivera-Pérez, J.A. (2018). Streamlined ex vivo and in vivo genome editing in mouse embryos using recombinant adeno-associated viruses. Nat. Commun. *9*, 412. https://doi.org/10.1038/s41467-017-02706-7.
10. Nagano, M., Watson, D.J., Ryu, B.-Y., Wolfe, J.H., and Brinster, R.L. (2002). Lentiviral vector transduction of male germ line stem cells in mice. FEBS Lett. *524*, 111–115. https://doi.org/10.1016/s0014-5793(02)03010-7.
11. Kobayashi, T., Namba, M., Koyano, T., Fukushima, M., Sato, M., Ohtsuka, M., and Matsuyama, M. (2018). Successful production of genome-edited rats by the rGONAD method. BMC Biotechnol. *18*, 19. https://doi.org/10.1186/s12896-018-0430-5.
12. Fan, Z., Li, W., Lee, S.R., Meng, Q., Shi, B., Bunch, T.D., White, K.L., Kong, I.-K., and Wang, Z. (2014). Efficient gene targeting in golden Syrian hamsters by the CRISPR/Cas9 system. PLoS One *9*, e109755. https://doi.org/10.1371/journal.pone.0109755.
13. Hamra, F.K., Gatlin, J., Chapman, K.M., Grellhesl, D.M., Garcia, J.V., Hammer, R.E., and Garbers, D.L. (2002). Production of transgenic rats by lentiviral transduction of male germ-line stem cells. Proc. Natl. Acad. Sci. USA *99*, 14931–14936. https://doi.org/10.1073/pnas.222561399.
14. Dewsbury, D.A., and Lanier, D.L. (1976). Effects of variations in copulatory behavior on pregnancy in two species of Peromyscus. Physiol. Behav. *17*, 921–924. https://doi.org/10.1016/0031-9384(76)90009-3.
15. Bedford, N.L., and Hoekstra, H.E. (2015). Peromyscus mice as a model for studying natural variation. eLife *4*, e06813. https://doi.org/10.7554/eLife.06813.
16. Hartung, T.G., and Dewsbury, D.A. (1978). A Comparative Analysis of Copulatory Plugs in Muroid Rodents and Their Relationship to Copulatory Behavior. J. Mammal. *59*, 717–723. https://doi.org/10.2307/1380136.
17. Dewsbury, D.A., Estep, D.Q., and Lanier, D.L. (1977). Estrous cycles of nine species of muroid rodents. J. Mammal. *58*, 89–92.
18. Choi, J.K., and He, X. (2013). In vitro maturation of cumulus-oocyte complexes for efficient isolation of oocytes from outbred deer mice. PLoS One *8*, e56158. https://doi.org/10.1371/journal.pone.0056158.
19. Veres, M., Duselis, A.R., Graft, A., Pryor, W., Crossland, J., Vrana, P.B., and Szalai, G. (2012). The biology and methodology of assisted reproduction in deer mice (Peromyscus maniculatus). Theriogenology *77*, 311–319. https://doi.org/10.1016/j.theriogenology.2011.07.044.
20. Lee, S.T., Kim, T.M., Cho, M.Y., Moon, S.Y., Han, J.Y., and Lim, J.M. (2005). Development of a hamster superovulation program and adverse effects of gonadotropins on microfilament formation during oocyte development. Fertil. Steril. *83*, 1264–1274. https://doi.org/10.1016/j.fertnstert.2004.09.039.
21. Keebaugh, A.C., Modi, M.E., Barrett, C.E., Jin, C., and Young, L.J. (2012). Identification of variables contributing to superovulation efficiency for production of transgenic prairie voles (Microtus ochrogaster). Reprod. Biol. Endocrinol. *10*, 54. https://doi.org/10.1186/1477-7827-10-54.
22. Lo, N.-W., Chang, H.-T., and Wang, M.-T. (2009). Automatic Detection of Mouse Mating Behavior by Video Surveillance. In Proceedings: APSIPA ASC 2009 : Asia-Pacific Signal and Information Processing Association, 2009 Annual Summit and Conference, pp. 668–671.
23. Doroba, C.K., and Sears, K.E. (2010). The divergent development of the apical ectodermal ridge in the marsupial Monodelphis domestica. Anat. Rec. *293*, 1325–1332. https://doi.org/10.1002/ar.21183.
24. Buchthal, J., Evans, S.W., Lunshof, J., Telford, S.R., 3rd, and Esvelt, K.M. (2019). Mice Against Ticks: an experimental community-guided effort to prevent tick-borne disease by altering the shared environment. Philos. Trans. R. Soc. Lond. B Biol. Sci. *374*, 20180105. https://doi.org/10.1098/rstb.2018.0105.
25. Markoulaki, S., Meissner, A., and Jaenisch, R. (2008). Somatic cell nuclear transfer and derivation of embryonic stem cells in the mouse. Methods *45*, 101–114. https://doi.org/10.1016/j.ymeth.2008.04.002.
26. Soldner, F., Hockemeyer, D., Beard, C., Gao, Q., Bell, G.W., Cook, E.G., Hargus, G., Blak, A., Cooper, O., Mitalipova, M., et al. (2009). Parkinson's disease patient-derived induced pluripotent stem cells free of viral reprogramming factors. Cell *136*, 964–977. https://doi.org/10.1016/j.cell.2009.02.013.
27. Chu, V.T., Weber, T., Graf, R., Sommermann, T., Petsch, K., Sack, U., Volchkov, P., Rajewsky, K., and Kühn, R. (2016). Efficient generation of Rosa26 knock-in mice using CRISPR/Cas9 in C57BL/6 zygotes. BMC Biotechnol. *16*, 4. https://doi.org/10.1186/s12896-016-0234-4.
28. Utt, D.A. The Role of Olfaction in Mediation of Pregnancy Block in White-Footed Mice, Peromyscus leucopus noveboracencis. (1984). Dissertations, Theses, and Masters Projects. Paper 1539625244. https://doi.org/10.21220/s2-mcjn-yw40
29. Weinert, D., Waterhouse, J., and Nevill, A. (2004). Changes of Body Temperature and Thermoregulation in the Course of the Ovarian Cycle in Laboratory Mice. Biol. Rhythm Res. *35*, 171–185. https://doi.org/10.1080/09291010412331335724.
30. Marrone, B.L., Gentry, R.T., and Wade, G.N. (1976). Gonadal hormones and body temperature in rats: effects of estrous cycles, castration and steroid replacement. Physiol. Behav. *17*, 419–425. https://doi.org/10.1016/0031-9384(76)90101-3.
31. Smarr, B.L., Zucker, I., and Kriegsfeld, L.J. (2016). Detection of Successful and Unsuccessful Pregnancies in Mice within Hours of Pairing through Frequency Analysis of High Temporal Resolution Core Body Temperature Data. PLoS One *11*, e0160127. https://doi.org/10.1371/journal.pone.0160127.
32. Byers, S.L., Wiles, M.V., Dunn, S.L., and Taft, R.A. (2012). Mouse estrous cycle identification tool and images. PLoS One *7*, e35538. https://doi.org/10.1371/journal.pone.0035538.
33. Clark, F.H. (1938). Age of Sexual Maturity in Mice of the Genus Peromyscus. J. Mammal. *19*, 230–234. https://doi.org/10.2307/1374620.
34. Lee, M., Ahn, J.I., Lee, A.R., Ko, D.W., Yang, W.S., Lee, G., Ahn, J.Y., and Lim, J.M. (2017). Adverse Effect of Superovulation Treatment on Maturation, Function and Ultrastructural Integrity of Murine Oocytes. Mol. Cells *40*, 558–566. https://doi.org/10.14348/molcells.2017.0058.
35. Ertzeid, G., and Storeng, R. (2001). The impact of ovarian stimulation on implantation and fetal development in mice. Hum. Reprod. *16*, 221–225. https://doi.org/10.1093/humrep/16.2.221.
36. Davis, S.W., and Keisler, J.L. (2016). Embryonic Development of the Deer Mouse, Peromyscus maniculatus. PLoS One *11*, e0150598. https://doi.org/10.1371/journal.pone.0150598.
37. Wollnik, F., and Turek, F.W. (1988). Estrous correlated modulations of circadian and ultradian wheel-running activity rhythms in LEW/Ztm rats. Physiol. Behav. *43*, 389–396. https://doi.org/10.1016/0031-9384(88)90204-1.
38. Wollnik, F., and Döhler, K.D. (1986). Effects of adult or perinatal hormonal environment on ultradian rhythms in locomotor activity of laboratory LEW/Ztm rats. Physiol. Behav. *38*, 229–240. https://doi.org/10.1016/0031-9384(86)90158-7.
39. Slonaker, J.R. (1924). THE EFFECT OF PUBESCENCE, OESTRUATION AND MENOPAUSE ON THE VOLUNTARY ACTIVITY IN THE ALBINO RAT. American Journal of Physiology-Legacy Content *68*, 294–315. https://doi.org/10.1152/ajplegacy.1924.68.2.294.
40. Matikainen-Ankney, B.A., Garmendia-Cedillos, M., Ali, M., Krynitsky, J., Salem, G., Miyazaki, N.L., Pohida, T., and Kravitz, A.V. (2019). Rodent activity detector (RAD), an open source device for measuring activity in rodent home cages. eNeuro *6*, ENEURO.0160–19.2019. https://doi.org/10.1523/ENEURO.0160-19.2019.
41. Valientes, D.A., Raus, A.M., and Ivy, A.S. (2021). An improved method for individual tracking of voluntary wheel running in pair-housed juvenile mice. Bio. Protoc. *11*, e4071. https://doi.org/10.21769/BioProtoc.4071.

42. Prendergast, B.J., Beery, A.K., Paul, M.J., and Zucker, I. (2012). Enhancement and suppression of ultradian and circadian rhythms across the female hamster reproductive cycle. J. Biol. Rhythms *27*, 246–256. https://doi.org/10.1177/0748730412441315.

43. Paull, J.A., and Fairbrother, A. (1985). Pregnancy diagnosis by vaginal lavage in deer mice,Peromyscus maniculatus. J. Exp. Zool. *233*, 143–149. https://doi.org/10.1002/jez.1402330121.

44. Cora, M.C., Kooistra, L., and Travlos, G. (2015). Vaginal Cytology of the Laboratory Rat and Mouse: Review and Criteria for the Staging of the Estrous Cycle Using Stained Vaginal Smears. Toxicol. Pathol. *43*, 776–793. https://doi.org/10.1177/0192623315570339.

45. Wolcott, N.S., Sit, K.K., Raimondi, G., Hodges, T., Shansky, R.M., Galea, L.A.M., Ostroff, L.E., and Goard, M.J. (2022). Automated classification of estrous stage in rodents using deep learning. Sci. Rep. *12*, 17685. https://doi.org/10.1038/s41598-022-22392-w.

46. Selvaraju, R.R., Cogswell, M., Das, A., Vedantam, R., Parikh, D., and Batra, D. (2017). Grad-CAM: Visual Explanations from Deep Networks via Gradient-Based Localization. In 2017 IEEE International Conference on Computer Vision (ICCV) (IEEE), pp. 618–626. https://doi.org/10.1109/ICCV.2017.74.

47. Shi, Y., Pulliam, D.A., Liu, Y., Hamilton, R.T., Jernigan, A.L., Bhattacharya, A., Sloane, L.B., Qi, W., Chaudhuri, A., Buffenstein, R., et al. (2013). Reduced mitochondrial ROS, enhanced antioxidant defense, and distinct age-related changes in oxidative damage in muscles of long-lived Peromyscus leucopus. Am. J. Physiol. Regul. Integr. Comp. Physiol. *304*, R343–R355. https://doi.org/10.1152/ajpregu.00139.2012.

48. Sacher, G.A., and Hart, R.W. (1978). Longevity, aging and comparative cellular and molecular biology of the house mouse, Mus musculus, and the white-footed mouse, Peromyscus leucopus. Birth Defects Orig. Artic. Ser. *14*, 71–96.

49. Dixon, D., Alison, R., Bach, U., Colman, K., Foley, G.L., Harleman, J.H., Haworth, R., Herbert, R., Heuser, A., Long, G., et al. (2014). Nonproliferative and proliferative lesions of the rat and mouse female reproductive system. J. Toxicol. Pathol. *27*, 1S–107S. https://doi.org/10.1293/tox.27.1S.

50. Westwood, F.R. (2008). The female rat reproductive cycle: a practical histological guide to staging. Toxicol. Pathol. *36*, 375–384. https://doi.org/10.1177/0192623308315665.

51. Gaytan, F., Morales, C., Leon, S., Heras, V., Barroso, A., Avendaño, M.S., Vazquez, M.J., Castellano, J.M., Roa, J., and Tena-Sempere, M. (2017). Development and validation of a method for precise dating of female puberty in laboratory rodents: The puberty ovarian maturation score (Pub-Score). Sci. Rep. *7*, 46381. https://doi.org/10.1038/srep46381.

52. Sun, Y., Desierto, M.J., Ueda, Y., Kajigaya, S., Chen, J., and Young, N.S. (2014). Peromyscus leucopus mice: a potential animal model for haematological studies. Int. J. Exp. Pathol. *95*, 342–350. https://doi.org/10.1111/iep.12091.

53. Horvath, S., Haghani, A., Zoller, J.A., Naderi, A., Soltanmohammadi, E., Farmaki, E., Kaza, V., Chatzistamou, I., and Kiaris, H. (2022). Methylation studies in Peromyscus: aging, altitude adaptation, and monogamy. GeroScience *44*, 447–461. https://doi.org/10.1007/s11357-021-00472-5.

54. O'Neal, T.J., Friend, D.M., Guo, J., Hall, K.D., and Kravitz, A.V. (2017). Increases in physical activity result in diminishing increments in daily energy expenditure in mice. Curr. Biol. *27*, 423–430. https://doi.org/10.1016/j.cub.2016.12.009.

55. Novak, C.M., Burghardt, P.R., and Levine, J.A. (2012). The use of a running wheel to measure activity in rodents: relationship to energy balance, general activity, and reward. Neurosci. Biobehav. Rev. *36*, 1001–1014. https://doi.org/10.1016/j.neubiorev.2011.12.012.

56. Eleftheriou, B.E., Bronson, F.H., and Zarrow, M.X. (1962). Interaction of olfactory and other environmental stimuli on implantation in the deer mouse. Science *137*, 764. https://doi.org/10.1126/science.137.3532.764.

57. Holzenberger, M., Dupont, J., Ducos, B., Leneuve, P., Géloën, A., Even, P.C., Cervera, P., and Le Bouc, Y. (2003). IGF-1 receptor regulates lifespan and resistance to oxidative stress in mice. Nature *421*, 182–187. https://doi.org/10.1038/nature01298.

58. Liang, H., Masoro, E.J., Nelson, J.F., Strong, R., McMahan, C.A., and Richardson, A. (2003). Genetic mouse models of extended lifespan. Exp. Gerontol. *38*, 1353–1364. https://doi.org/10.1016/j.exger.2003.10.019.

59. Kim, E.B., Fang, X., Fushan, A.A., Huang, Z., Lobanov, A.V., Han, L., Marino, S.M., Sun, X., Turanov, A.A., Yang, P., et al. (2011). Genome sequencing reveals insights into physiology and longevity of the naked mole rat. Nature *479*, 223–227. https://doi.org/10.1038/nature10533.

60. McGraw, L.A., and Young, L.J. (2010). The prairie vole: an emerging model organism for understanding the social brain. Trends Neurosci. *33*, 103–109. https://doi.org/10.1016/j.tins.2009.11.006.

61. Eimer, W.A., and Vassar, R. (2013). Neuron loss in the 5XFAD mouse model of Alzheimer's disease correlates with intraneuronal Aβ42 accumulation and Caspase-3 activation. Mol. Neurodegener. *8*, 2. https://doi.org/10.1186/1750-1326-8-2.

62. Tian, C., Hromatka, B.S., Kiefer, A.K., Eriksson, N., Noble, S.M., Tung, J.Y., and Hinds, D.A. (2017). Genome-wide association and HLA region fine-mapping studies identify susceptibility loci for multiple common infections. Nat. Commun. *8*, 599. https://doi.org/10.1038/s41467-017-00257-5.

63. Noble, C., Min, J., Olejarz, J., Buchthal, J., Chavez, A., Smidler, A.L., DeBenedictis, E.A., Church, G.M., Nowak, M.A., and Esvelt, K.M. (2019). Daisy-chain gene drives for the alteration of local populations. Proc. Natl. Acad. Sci. USA *116*, 8275–8282. https://doi.org/10.1073/pnas.1716358116.

64. Min, J., Noble, C., Najjar, D., and Esvelt, K.M. (2017). Daisy quorum drives for the genetic restoration of wild populations. Preprint at bioRxiv. https://doi.org/10.1101/115618.

65. Schaible, U.E., Kramer, M.D., Eichmann, K., Modolell, M., Museteanu, C., and Simon, M.M. (1990). Monoclonal antibodies specific for the outer surface protein A (OspA) of Borrelia burgdorferi prevent Lyme borreliosis in severe combined immunodeficiency (scid) mice. Proc. Natl. Acad. Sci. USA *87*, 3768–3772. https://doi.org/10.1073/pnas.87.10.3768.

66. Hasegawa, A., Mochida, K., Matoba, S., Yonezawa, K., Ohta, A., Watanabe, G., Taya, K., and Ogura, A. (2012). Efficient production of offspring from Japanese wild-derived strains of mice (Mus musculus molossinus) by improved assisted reproductive technologies. Biol. Reprod. *86*, 167. https://doi.org/10.1095/biolreprod.111.098491.

67. Hasegawa, A., Mochida, K., Nakamura, A., Miyagasako, R., Ohtsuka, M., Hatakeyama, M., and Ogura, A. (2022). Use of anti-inhibin monoclonal antibody for increasing the litter size of mouse strains and its application to in vivo-genome editing technology. Biol. Reprod. *107*, 605–618. https://doi.org/10.1093/biolre/ioac068.

68. Mochida, K., Morita, K., Sasaoka, Y., Morita, K., Endo, H., Hasegawa, A., Asano, M., and Ogura, A. (2024). Superovulation with an anti-inhibin monoclonal antibody improves the reproductive performance of rat strains by increasing the pregnancy rate and the litter size. Sci. Rep. *14*, 8294. https://doi.org/10.1038/s41598-024-58611-9.

69. Li, W., Wei, W., Zhu, S., Zhu, J., Shi, Y., Lin, T., Hao, E., Hayek, A., Deng, H., and Ding, S. (2009). Generation of rat and human induced pluripotent stem cells by combining genetic reprogramming and chemical inhibitors. Cell stem cell *4*, 16–19. https://doi.org/10.1016/j.stem.2008.11.014.

70. Li, W., Zhou, H., Abujarour, R., Zhu, S., Young Joo, J., Lin, T., Hao, E., Schöler, H.R., Hayek, A., and Ding, S. (2009). Generation of human-induced pluripotent stem cells in the absence of exogenous Sox2. Stem cells (Dayton. Ohio) *27*, 2992–3000. https://doi.org/10.1002/stem.240.

71. Buehr, M., Meek, S., Blair, K., Yang, J., Ure, J., Silva, J., McLay, R., Hall, J., Ying, Q.-L., and Smith, A. (2008). Capture of authentic embryonic stem cells from rat blastocysts. Cell *135*, 1287–1298. https://doi.org/10.1016/j.cell.2008.12.007.

72. Hockemeyer, D., Soldner, F., Cook, E.G., Gao, Q., Mitalipova, M., and Jaenisch, R. (2008). A drug-inducible system for direct reprogramming of human somatic cells to pluripotency. Cell stem cell *3*, 346–353. https://doi.org/10.1016/j.stem.2008.08.014.

73. Gage, G.J., Kipke, D.R., and Shain, W. (2012). Whole animal perfusion fixation for rodents. J. Vis. Exp. *65*, 3564. https://doi.org/10.3791/3564.

74. Johnson, J., DelGiudice, B., Bangari, D., Peterson, E., Ulinski, G., Ryan, S., and Thurberg, B. (2019). The Laboratory Mouse, 1st Edition (CRC Press). https://doi.org/10.1201/9780429057755.

75. Chanut, F.J.A., and Williams, A.M. (2016). The Syrian Golden Hamster Estrous Cycle: Unique Characteristics, Visual Guide to Staging, and Comparison with the Rat. Toxicol. Pathol. *44*, 43–50. https://doi.org/10.1177/0192623315607668.

76. Willson, G., and Cimon, K.Y. (2023). Ovary - Atrophy. National Toxicology Program Nonneoplastic Lesion Atlas. https://ntp.niehs.nih.gov/atlas/nnl/reproductive-system-female/ovary/Atrophy.

77. Woźna-Wysocka, M., Rybska, M., Błaszak, B., Jaśkowski, B.M., Kulus, M., and Jaśkowski, J.M. (2021). Morphological changes in bitches endometrium affected by cystic endometrial hyperplasia - pyometra complex - the value of histopathological examination. BMC Vet. Res. *17*, 174. https://doi.org/10.1186/s12917-021-02875-0.

STAR★METHODS

KEY RESOURCES TABLE

REAGENT or RESOURCE	SOURCE	IDENTIFIER
Antibodies		
Oct4 antibody	Santa Cruz Biotechnology	Cat# sc-9081
Sox2 antibody	R&D Biosystems	Cat# MAB2018R
Nanog antibody	Thermo Fisher Scientific (Bethyl Laboratories)	Cat# A300-398A
Chemicals, peptides, and recombinant proteins		
Pregnant Mare Serum Gonadotropin (PMSG)	ProSpec-Tany TechnoGene Ltd.	Cat# HOR-272
Human Chorionic Gonadotropin (hCG)	ProSpec-Tany TechnoGene Ltd.	Cat# HOR-250
Dulbecco's Modified Eagle Medium (DMEM)	Thermo Fisher Scientific (Gibco)	Cat# 11965092
Fetal Bovine Serum (FBS)	Thermo Fisher Scientific (Gibco)	Cat# A5670701
Penicillin-Streptomycin (Pen/Strep)	Thermo Fisher Scientific (Gibco)	Cat# 15140148
GlutaMAX (100×)	Thermo Fisher Scientific (Gibco)	Cat# 35050061
Tyrode′s Solution, Acidic	MilliporeSigma (Sigma-Aldrich)	Cat# T1788
Trypsin-EDTA (0.25%)	Thermo Fisher Scientific (Gibco)	Cat# 25200056
KnockOut DMEM	Thermo Fisher Scientific (Gibco)	Cat# 10829018
KnockOut™ Serum Replacement (KSR)	Thermo Fisher Scientific (Gibco)	Cat #10828028
LIF (ESGRO® mLIF)	MilliporeSigma (Sigma-Aldrich)	Cat# ESG1106
MEM Non-Essential Amino Acids	Thermo Fisher Scientific (Gibco)	Cat# 11140050
β-Mercaptoethanol	MilliporeSigma (Sigma-Aldrich)	Cat# M6250
DMEM/F-12	Thermo Fisher Scientific (Gibco)	Cat#11320033
Neurobasal medium	Thermo Fisher Scientific (Gibco)	Cat# 21103049
N-2 Supplement (100×)	Thermo Fisher Scientific (Gibco)	Cat# 17502048
B-27 Supplement (50×)	Thermo Fisher Scientific (Gibco)	Cat# 17504044
GSK3β	Li et al.[69]; Li et al.[70]; Buehr et al.[71]	N/A
ERK/MEK	Li et al.[69]; Li et al.[70]; Buehr et al.[71]	N/A
StemPro™ Accutase™ Cell Dissociation Reagent	Thermo Fisher Scientific (Gibco)	Cat# A1110501
TrypLE™ Express Enzyme	Thermo Fisher Scientific (Gibco)	Cat# 12604013
Collagenase, Type IV, powder	Thermo Fisher Scientific (Gibco)	Cat# 17104019
Pronase (neutral protease)	MilliporeSigma (Sigma-Aldrich)	Cat# 537088
Versene Solution	Thermo Fisher Scientific (Gibco)	Cat# 15040066
Dispase II	Thermo Fisher Scientific (Gibco)	Cat# 17105041
ReLeSR	STEMCELL Technologies	N/A
Mitomycin C	MilliporeSigma (Sigma-Aldrich)	Cat# 10107409001
Corning® Matrigel® hESC-Qualified Matrix	MilliporeSigma (Sigma-Aldrich)	Cat# CLS354277
Gelatin	MilliporeSigma (Sigma-Aldrich)	Cat# G1890
4% Paraformaldehyde in PBS	Fisher Scientific	Cat# 50-259-98
Phosphate-Buffered Saline (PBS), 1×	Corning	Cat# 21-040-CV
Triton X-100	MilliporeSigma (Sigma-Aldrich)	Cat# T8787
Wescodyne® disinfectant	Penetone Corporation	N/A
Doxycycline (Dox)	MilliporeSigma (Sigma-Aldrich)	D9891
Alt-R CRISPR-Cas9 sgRNA	Integrated DNA Technologies (IDT)	N/A
Alt-R S.p. Cas9 Nuclease V3	Integrated DNA Technologies (IDT)	Cat #1081059

(*Continued on next page*)

Continued

REAGENT or RESOURCE	SOURCE	IDENTIFIER
PrimeSTAR® DNA Polymerase	Takara Bio	Cat# R050A
Ketamine Hydrochloride Injection, 100 mg/mL	Dechra Veterinary Products LLC	NDC 17033-101-10
Xylazine Hydrochloride Injection (AnaSed®), 20 mg/mL	Akorn, Inc.	NDC 59399-110-20
Acepromazine maleate injection, 10 mg/mL (PromAce®)	Boehringer Ingelheim Animal Health USA Inc.	NDC 0010-3827-01
M2 Medium (with BSA & phenol red)	CytoSpring	Cat# M2113
KSOM medium (with BSA & phenol red)	CytoSpring	Cat# K0113
EmbryoMax Filtered Light Mineral Oil	MilliporeSigma (Sigma-Aldrich)	Cat#: ES-005-C
Methanol	Volu-Sol	Cat# VMT-032
Isoflurane, Inhalation USP	Patterson Veterinary (Piramal Healthcare)	Cat# 07-890-8115
10% Neutral Buffered Formalin	Avantik	Cat# RS4061
Paraffin Wax (Surgipath Paraplast X-tra)	Leica Biosystems	Cat# 39603002
SelecTech Hematoxylin 560 MX	Leica Biosystems	Cat# 3801575
SelecTech Alcoholic Eosin Y 515	Leica Biosystems	Cat# 3801616
Tissue-Tek® O.C.T. Compound	Sakura Finetek USA, Inc.	Cat# 4583
Critical commercial assays		
Guide-it Long ssDNA Production System v2	Takara Bio	Cat# 632666
GenElute Mammalian Genomic DNA Miniprep Kit	MilliporeSigma (Sigma-Aldrich)	Cat# G1N70
SQK-LSK-112 Ligation Sequencing Kit	Oxford Nanopore Technologies	Cat# SQK-LSK-112
Epredia Three-Step Stain Kit	Epredia (Richard-Allan Scientific)	Cat# 3300
Deposited data		
Nanopore sequencing reads used for genotyping	This paper	PRJNA1364316
Peromyscus leucopus genome assembly	This paper	JBSIEY000000000
Experimental models: Cell lines		
HEK 293T cells	ATCC	RRID: CVCL_0063
Experimental models: Organisms/strains		
Peromyscus leucopus	Gift from Dr. Sam R. Telford, Tufts University	N/A
DR-4 transgenic mice	The Jackson Laboratory	Strain #:003208; RRID: IMSR_JAX:003208
NSG mice (SCID mice)	The Jackson Laboratory	Strain #:005557; RRID: IMSR_JAX:005557
C57BL/6 mice	Charles River Laboratories	Strain Code: 027
LVG Golden Syrian Hamster (Mesocricetus auratus)	Charles River Laboratories	Strain code: 049
Recombinant DNA		
Lentiviral vectors (Dox-inducible, expressing hOct3/4, hSox2, hc-Myc, hKlf4, and tTA)	Hockemeyer et al.[72]	Addgene Plasmids: 20726, 20725, 20724, 20723, 20342
Software and algorithms		
Raspberry Pi OS (formerly known as Raspbian)	Raspberry Pi Foundation	N/A
OpenCV (Open Source Computer Vision Library)	opencv.org/PyPI	RRID: SCR_015526
PostgreSQL (relational database)	postgresql.org	N/A
BGSLibrary	BGSLibrary/pybgs (Python)	N/A
statsmodels Python package	Python Software Foundation	RRID: SCR_016074
ImageJ (image analysis software)	NIH	RRID: SCR_003070

(*Continued on next page*)

Continued

REAGENT or RESOURCE	SOURCE	IDENTIFIER
ResNet-50 (pre-trained model)	PyTorch	N/A
Camera-based activity tracking and analysis code (archival version)	This paper	GitHub: https://github.com/Buchthal/Peromyscus_Transgenesis; Zenodo: https://doi.org/10.5281/zenodo.17622641
Other		
Eclipse Ti-E	Nikon	N/A
4D-Nucleofector	Lonza	N/A
NEPA21 Electro-Kinetic Transfection System	Bulldog Bio, Inc.	N/A
G2 E-Mitter telemetry implant	Starr Life Sciences Corp.	N/A
Raspberry Pi Zero 2 W	Raspberry Pi Foundation	N/A
Raspberry Pi NoIR Camera V2 module	Raspberry Pi Foundation	N/A
Raspberry Pi Zero case	Raspberry Pi Foundation	N/A
Coated VICRYL® suture, 5-0, 18″, C-3 needle (violet braided)	Ethicon	Cat# J385H
Eppendorf FemtoJet 4i microinjector	Caliber Scientific	Cat# 5252000021
PromethION sequencing system	Oxford Nanopore Technologies	RRID: SCR_017987
PromethION R9.4 flow cell	Oxford Nanopore Technologies	Cat# FLO-PRO002
FLIR Lepton 3.5	Teledyne FLIR	Cat# 500-0771-01
PureThermal 3 USB adapter	GroupGets	Cat# PURETHERMAL-3
Nylon flocked swabs	SNT Biotech	Cat# SNT-ORALSWAB-500
TissueFAXS SL Q confocal scanner (10×)	TissueGnostics USA	N/A
Aperio AT2 digital slide scanner (20×)	Leica Biosystems	RRID: SCR_021256

EXPERIMENTAL MODEL AND STUDY PARTICIPANT DETAILS

Peromyscus leucopus breeding colony

Peromyscus were from a closed, specific pathogen free outbred colony at Tufts University School of Veterinary Medicine. This colony originated at the Harvard School of Public Health from wild mice trapped during 1993 from Martha's Vineyard, MA, and Spooner, WI, and comprise a golden coat color mutant. Mice from the Tufts colony were in their 30th generation when transferred. At MIT, mice were maintained in harem breeding trios, with each cage containing no more than three adults plus weanlings.

All animal procedures were approved by the appropriate IACUCs: *Peromyscus* (MIT), *Mus musculus* (Harvard University), and hamster (Tufts University). Animals were maintained at each institution in accordance with institutional protocols and DoD guidelines.

METHOD DETAILS

Superovulation of *Peromyscus*

The following super-ovulation protocol was created by the Fisher lab and given to the Esvelt lab via personal communication. Briefly, 4 to 6-week-old female *P. leucopus* were injected intraperitoneally with 20 IU of PMSG 1 h prior to lights out followed by 20 IU of hCG 72 or 48 h later. Mice were mated overnight and then embryos were harvested from donor females 36 h after timed matings were set up.

Mus embryonic fibroblast derivation (feeders)

For MEF isolation, embryos were isolated at E13.5 from DR-4 transgenic mice and the fibroblast-containing tissue was collected under a dissection scope. The collected tissues were physically dissociated and incubated in Trypsin at 37°C for 20 min after which cells were resuspended in MEF medium, γ-irradiated, and frozen for later use.

pESC derivation

For pESC derivation, 8-cell embryos were extracted at E3.0 from *Peromyscus* and plated in 96-well plates that had been coated with a *Mus* embryonic fibroblast feeder layer. pESC derivation media conditions are detailed in Figure S1C. MEFs were pre-plated at least 12 h in advance in MEF medium (DMEM supplemented with 10% fetal bovine serum, 1× penicillin-streptomycin, and 2 mM GlutaMAX). In preparation for the blastocyst plating, MEF medium was removed from the 96-well plates with feeders and replaced

with 500 μL of pESC-derivation medium. Immediately prior to plating, the zona surrounding the blastocyst was removed by brief exposure to acid Tyrode's solution. After zona removal, single blastocysts were placed in wells of 4-well plates, which were placed in a CO2 incubator and allowed to attach to the feeder layers. When an inner cell mass outgrowth was observed (5–6 days after plating), cells were first passaged using trypsin–EDTA. After a brief incubation at 37°C, cells were dissociated by pipetting up and down 3–4 times. After another short incubation, the contents of the wells were then transferred into a 12-well plate with feeders in the presence of pESC-derivation medium and further cultured.

- **Attempt 1 details:** In brief, using mESCD-KSR (KnockOut DMEM supplemented with 15% KnockOut Serum Replacement, 1,000 U/mL LIF, 1× MEM Non-Essential Amino Acids, 2 mM GlutaMAX, and 0.1 mM β-mercaptoethanol), the Zona Pellucida was removed from two blastocysts at E5.5 and embryos were plated individually on *Mus* embryonic fibroblast (MEF)-coated plates with mESCD-KSR.
- **Attempt 2 details:** including mESCD-KSR-2i, both with and without N2B27 (a serum-free, chemically defined mixture of DMEM/F-12 and Neurobasal medium supplemented with N-2 and B-27) (Figure S1C), next added 2i, a selective small molecule inhibitor of differentiation-inducing signals from GSK3β and ERK/MEK, to our mESCD-KSR medium. In our second attempt, only one blastocyst plated in the mESCD-KSR-2i condition formed an expanded outgrowth, which carried over, but never gave rise to a stable line. Next, we supplemented mESCD-KSR-2i with N2B27 which was previously found to facilitate ESC derivation in rats[71] Our most promising results came from our final attempt: out of the 9 blastocysts plated in mESCD-KSR-2i, all we plated 9 blastocysts in mESCD-KSR-2i, the same condition as our second attempt. All nine outgrowths formed large outgrowths and five gave rise to ESC-like colonies that became stable lines.

pESC dissociation and propagation challenges

Due to challenges associated with pESC propagation, our *Peromyscus* ESC-like colonies were not easy to maintain; grew slowly, differentiated frequently and were not ready to dissociate for 7–10 days after plating. Some colonies appeared to be resistant to dissociation, forming large clumps even after long incubations in Trypsin or Accutase. We employed a variety of dissociation reagents without detectable improvement, including higher concentration of Trypsin, higher concentration of EDTA in Trypsin, TrypIE Express, Collagenase, Pronase, Versene Solution, Dispase, ReLeSR, as well as manual passaging. Moreover, MEFs appeared to be unhealthy, during the prolonged periods in culture between passages. Swapping MEFs inactivated by irradiation with Mitomycin C inactivated MEFs did not result in noticeable improvement. Using a lower density of MEFs alleviated some of the problems associated with higher density (including lifting off plates while trapping pESCs) but did not sufficiently support pESC propagation. We also tried culturing pESCs in the absence of MEFs by coating our plates with Matrigel or Gelatin, but most cells either didn't attach or formed spheres/embryoid bodies that could not be dissociated. Due to aforementioned challenges, including spontaneous differentiation and issues with dissociation and inefficient propagation, further optimization of culture conditions is needed in order to facilitate pESC based transgenesis methods.

pESC staining

Cells were fixed in 4% paraformaldehyde for 20 min at 25°C, washed three times with PBS, and blocked for 15 min with 5% FBS in PBS containing 0.1% Triton X-. After incubation with primary antibodies against Oct4 (Santa Cruz H-134); Sox2 (R&D Biosystems); Nanog (Bethyl A300-398A); for 1 h in 1% FBS in PBS containing 0.1% Triton X-, cells were washed three times with PBS and incubated with fluorophore-labeled appropriate secondary antibodies purchased from Jackson Immunoresearch. Cells were analyzed on a Nikon Eclipse Ti-E inverted microscope.

Teratoma formation

Teratoma formation was performed by depositing 1 × 10 ^6 cells under the flanks of recipient SCID mice (NSG mice). Tumors were isolated 3–6 weeks later for histological analysis. Mice were sacrificed before tumor size exceeded 1.5 cm in diameter.

Generations of *Peromyscus* tail tip fibroblasts

To generate primary fibroblasts for iPSC derivation, mice were sacrificed and a 1–2 mm piece tail was removed from 5 to 6 week old rodents. The tail tissue was then rinsed with Wescodyne (iodine-based antimicrobial solution) followed by 70% ethanol, and rinsed 2× in PBS with 1× Penstrep (Gibco). Working in a 6cm TC dish under a laminar flow hood, each tail biopsy was then finely minced with a sterile razor blade/scalpel into a 0.25mL mixture of collagenase and dispase neutral protease (4mg/mL each in DMEM). After mincing finely, 0.25 mL collagenase mixture was added to the plate, and incubated for 30 min at 37°C. Following dissociation, 6mLs of MEF media (DMEM +10%FBS + pen/strep) was added to the 6 cm plate and incubated overnight at 37°C, 5% CO2. The following day, to further aid dissociation of any large pieces of tissue, remaining tissue was titrated with a sterile Pasteur pipette. The tissue was then incubated for an additional 3 days at 37°C, 5% CO2 to allow cells to adhere and spread away from the tissue chunks. After 3–4 days, the media was refreshed, as cells began to undergo rapid proliferation. When nearly confluent, cells were passaged or frozen.

iPSC derivation

To create iPSCs, fully-differentiated adult somatic cells were returned to a pluripotent state using a cocktail of factors (hOct3/4, hSox2, hc-Myc, and hKlf4) that are known to maintain pluripotency during embryonic development. To generate *Peromyscus* iPSCs, the four factors, as well as the tetracycline transactivator, were delivered using tetracycline (Dox)-inducible lentiviral vectors. The lentiviral backbone for dox-inducible transgene expression was constructed by replacing the human ubiquitin C promoter of the FUW plasmid (Lois et al., 2002) with a tetracycline operator and minimal CMV promoter. For infections, virus was prepared by transfecting 293T cells with a mixture of viral plasmid and packaging constructs expressing the viral packaging functions and the VSV-G protein. Medium was replaced 24 h after transfection, and viral supernatants were collected at 48 and 72 h. After filtration, supernatants were pooled, and tail tip fibroblasts were incubated with viral supernatants and fresh media at a ratio of 1:1 for 24 h. They were subsequently cultured in ESC medium (KnockOut DMEM supplemented with 15% KnockOut Serum Replacement, 1,000 U/mL LIF, 1× non-essential amino acids, 2 mM GlutaMAX, and 0.1 mM β-mercaptoethanol). Fully reprogrammed colonies were passaged for 12–20 days, at which point Doxycycline was withdrawn. Unfortunately, spontaneous differentiation was observed following removal of Dox, indicating lack of successful reprogramming.

De novo sequencing of *Peromyscus* genome

Blood samples were collected in a collection tube coated with an anticoagulant (EDTA) and inverted 8–10 times immediately following collection to ensure proper mixing of the anticoagulant. Blood was shipped on dry ice immediately following extraction to Dovetail Genomics (Santa Cruz) for *de novo* genome assembly.

Guide targeting construct design & guide design

Rosa26 sgRNA for iGONAD and nuclear injection was purchased from Integrated DNA Technologies (Figure 2A). Rosa26 homology arms for ssDNA (for iGONAD) and targeting constructs (for nuclear injection) were identified by aligning the *Mus* Rosa26 locus to the *Peromyscus* genome assembled via Dovetail Genomics. Homology arms were synthesized as gBlocks via IDT and either cloned into a standard high copy number plasmid backbone, or used to make ssDNA, which was produced using the Guide-it Long ssDNA Production System v2 from Takara.

Electroporation of pESCs

1 × 10 ^7 cells were electroporated with 20 mg of DNA using a Lonza nucleofector and then seeded on MEFs.

Karyotyping

Live cells at passage 15 were sent to Cell Line Genetics for cytogenetic analysis. Analysis was performed on twenty G-banded metaphase male pESCs. Two abnormal male clones were analyzed. Clone 1 contained eighteen cells with trisomy 16 and trisomy 17. Clone 2 contains 2 cells which demonstrated trisomy 16.

I-GONAD

Mouse oviduct electroporation was performed as previously reported.[8] Briefly, 8–16 week old *Peromyscus* were mated with stud males and checked daily for sperm using vaginal lavage. If sperm was found, the female was subjected to iGONAD the same day. CRISPR gene editing cocktails were freshly assembled and contained 6 μM Cas9 protein (IDT 1081059, Lot # 0000405530), 30 μM gRNA, and 18 μM ssODNA (produced in-house). This cocktail was delivered into the oviduct of female mice through microcapillary injection. Oviduct electroporation was performed using a NEPA21 Electro-Kinetic Transfection System with a range of conditions including: Pd A: between 100 and 135 mA, Pd on: 5 msec, Pd off: 50 msec, three cycles, decay 10%.

Genotyping

The screening of founder pups was performed by PCR and direct sequencing using DNA obtained from ear slices. Genomic DNA was extracted from ear slices with the GenElute Mammalian Genomic DNA Mini-prep Kit (Sigma-Aldrich). PCR was performed with PrimeSTAR DNA Polymerase (Takara Bio) and the following primers *Rosa26-F (5′-GGGAGTTCTCTGCTGCCT-3′) and Rosa26-R (5′-AGTTTTGCTGCATAAAACCCC-3′)*.

Temperature & activity data monitoring

Data were gathered with G2 E-Mitter implants for core body temperature and locomotor activity (Starr Life Sciences Corp., Oakmont, PA). G2 E-Mitters were implanted in the abdominal cavity under anesthesia using a cocktail containing ketamine (150mg/kg), xylazine (5mg/kg) and acepromazine (2mg/kg). E-Mitters were sutured to the ventral muscle wall to maintain consistent core temperature measurements. Recordings began immediately, but mice were not mated until at least 3 estrous cycles were observed. Recordings were collected continuously at 1-min resolution for core body temperature and activity. All mice were between 10 and 16 weeks of age at the time of implant surgery and were handled once/wk across recordings at the time of cage changes, but otherwise were left undisturbed in single housing.

Leucopus mating set-up in estrous tracking experiments

Animals were maintained under 16:8 LD cycle of ~400 lux (light) to <1 lux red light (darkness), with lights on from 4a.m. to 8p.m. Food and water were available *ad libitum*. Mouse temperature and activity profiles were utilized to monitor estrous cycles remotely and mice were paired on the day of apparent estrus from 1 h before lights-off (7p.m.) to 5 h after lights-on the following day (9a.m.). Vaginal plugs were not monitored. Removal of the male was the only disturbance to the females besides weekly cage changes.

Mus musculus estrous tracking experiments

8 week old *Mus musculus* (C57BL/6) were maintained under 15:9 LD cycle of ~400 lux (light) to <1 lux red light (darkness), with lights on from 6a.m. to 9p.m. Food and water were available *ad libitum*. *Mus* activity profiles were used to monitor estrous cycles remotely. Cage changes were the only disturbance to the animals. To ensure robust cycling, bedding from a male cage was introduced at each cage change.

Hamster estrous tracking experiments

14 week old Syrian hamsters *Mesocricetus auratus* were maintained under 12:12 LD cycle of ~400 lux (light) to <1 lux red light (darkness), with lights on from 7a.m. to 7p.m. Food and water were available *ad libitum*. Hamster activity profiles were used to monitor estrous cycles remotely. Cage changes were the only disturbance to the animals.

Camera setup, data export & analysis

Each Raspberry Pi Zero 2 W was assigned a unique ID used to organize the data it processed. Each drive had a capacity of 32GB and was flashed with the Raspbian OS image and a script for startup configuration. The Raspberry Pi NoIR Camera V2 modules were connected to the Raspberry Pi Zero 2 W using a ribbon cable, and both were assembled into the official Raspberry Pi Zero case.

The Raspberry Pi systems were attached to acrylic stands using Command strips for ease of repositioning. The stands were placed next to each cage. For one experiment, near-IR (940nm), 100mA LEDs were attached to the stands and powered by the Raspberry Pi USB port to illuminate the mice at night.

Linux systemd utility was used to manage the image capture, processing and upload services. The image capture service captures 640 × 480 RGB images every 4 s using raspistill and saves them locally as jpegs. Every 10 min, the image processing service runs a Python program that uses OpenCV to compare each 2-tuple of consecutive images using the imagediff algorithm. Next, this service attempts to upload this data to a Postgres database in AWS RDS, then deletes the processed images to save storage. To mitigate network reliability issues, a copy of the data is written to a local file, to be recovered when the connection is restored. If enabled, the image upload service uploads stills to AWS S3, and inserts a corresponding row referencing the S3 URI into the database. Stills are stored until a successful upload, or until the disk reaches capacity.

All Raspberry Pis are connected to a VPN running on an AWS EC2 instance for remote debugging and to receive over-the-air software updates; other data was not sent over the VPN. Pis uploaded their IP address to S3 every 2 min, in part serving as a health check.

An AWS EC2 instance runs an alerting system as well as a web server for monitoring and data visualization. Every 6 h, a Python script checked that each Pi has uploaded its IP and data recently, and sent an email listing the Pis that have not. Every hour, the Raspberry Pi ID to mouse ID mapping was read from a Google Sheet and inserted into the database. Data was then downloaded from the database per mouse, grouped into 5-min windows, and stored in a day by window format. Further data processing in the form of outlier removal was available interactively on the web interface.

Vasectomies

Briefly, 8–12 week old male *Peromyscus* were anesthetized with a cocktail containing ketamine (150mg/kg), xylazine (5mg/kg) and acepromazine (2mg/kg) in preparation for surgery. Once anesthetized, the eyes were covered with ointment to prevent dryness and the abdomen was shaved with small clippers and cleaned with betadine followed by 70% ethanol, 3 times. Following aseptic technique, a small incision of about 1.5cm was made at a point level with the top of the legs. Another small incision was made in the body wall along the linea alba. With blunt forceps, the fat pad was pulled out, exposing the vas deferens. The vas deferens was cauterized with a high temperature cautery power handle. The fat pad was then reinserted inside the body wall, and repeated on the other side. The body wall was sutured with 1–2 stitches of coated VICRYL sutures and the skin was closed with wound clips which were removed 7–14 days later.

Embryo transfers

Briefly, 8–16 week old female *Peromyscus* were mated with vasectomized males on the night of apparent estrus to generate pseudopregnant recipients. The following day, females were anesthetized with a cocktail containing ketamine (150mg/kg), xylazine (5mg/kg) and acepromazine (2mg/kg) in preparation for surgery. Once anesthetized, the eyes were covered with eye ointment to prevent dryness and the lower back of the recipient mouse was shaved with small clippers. Using cotton tip applicators, the surgical area was cleaned with betadine followed by 70% ethanol, repeated 3 times. Following aseptic technique, a small transverse incision (less than 1cm) was made with fine dissecting scissors about 1cm to the right of the spinal cord at the level of the last rib. Once the ovary or fat pad could be visualized through the body wall, a small incision was made just over the ovary. With blunt fine forceps, the fat pad

was pulled through the incision and the ovary, oviduct and uterine horn was pulled out and laid down over the middle of the back, so that the oviduct was exposed outside the body wall. 4 manipulated or unmanipulated 2-cell embryos were transferred into the oviduct by puncturing the oviduct wall, in between the infundibulum and ampulla with a sterile 30g needle and transferring the embryos through the small opening. Once the embryos have been transferred, the ovary, oviduct and uterus were placed inside the body wall. The body wall was sutured with 1 or 2 stitches of coated VICRYL sutures and the skin was closed with wound clips, which were removed 7–14 days after embryo transfer.

Nuclear injection in two-cell stage embryos

Briefly, *Peromyscus* females were used as embryo donors and recipients. Camera-tracked donors were mated with proven studs. Two days later, 2-cell embryos were flushed from the oviducts using prewarmed M2 medium (CytoSpring; M2113). After embryo collection, 2-cell embryos were transferred to pre-equilibrated KSOM (CytoSpring; K0113) overlaid with mineral oil and incubated at 37°C (5% CO2 and 5% O2). SpCas9 protein (final concentration 50 ng/ul) and sgRNA (final concentration 50 ng/ul) were mixed and incubated at room temperature for 15–20 min. DNA template was added to the RNP solution at a final concentration of 10 ng/ul. For each 2-cell, the nucleus of each blastomere was injected. Pressure for microinjection was provided by Eppendorf FemtoJet 4i. *Peromyscus* females were mated to vasectomized *Peromyscus* males one day prior to 2-cell microinjection. The same day as microinjection, manipulated 2-cell embryos were transferred to pseudopregnant females' oviducts.

Nanopore sequencing

Genomic DNA was extracted using the GenElute Mammalian Genomic DNA Miniprep Kit (MilliporeSigma, Burlington, MA, USA). Samples containing 1 μg of genomic DNA were prepared for sequencing using the SQK-LSK-112 Ligation Sequencing Kit (Oxford Nanopore Technologies, Oxford, UK). Sequencing was performed on a PromethION system equipped with R9.4 flow cells (Oxford Nanopore Technologies, Oxford, UK). Adaptive sequencing targeted a 4 Mb region of CAG-EGFP insert flanked by R26 locus homology regions of equal lengths.

Image processing for *Mus* and hamsters

Still images captured every 4 s with a resolution of 640 × 480 were cropped to retain only the quadrant where food intake activities were observed. For *Mus*, only images from 0600 to 0900 UTC each day were used for downstream analysis. For hamsters, only images from 0000 to 0820 UTC were used. Each frame was then normalized to have a minimum of 0 and maximum of 255 in each of the 3 channels. "TwoPoint" background subtraction algorithm from Python package bgslibrary was then applied iteratively to each frame and a background learned and subtracted from each frame. These frames were then normalized to a range of 0–1, and L2 norms computed for each frame and stored in a separate array for each day. To reduce the impact of spurious activities, adjacent elements in this array above a threshold of T but forming blocks within the index range of (p,q) of less than N or more than N′ neighbors were replaced with the mean of elements with indices p-1 and q+1. For *Mus*, T = 25, *N* = 20, N' = 200. For hamsters, T = 15, *N* = 3, N' = 100. The differences between adjacent elements of this resulting array was then computed for each day and plotted as a heatmap. For heatmap visualization, a max and min normalization value was set using 30 break histogram binning. More specifically, a 30 bin histogram of the log10 difference was generated with 0 and 1 set just outside the tails. For the cumulative activity plots, activity levels for each time point were convolved with a kernel of one hundred ones, max pooled with a block size of 100 and the daily sum was plotted as time series bar plots. These cumulative activity values were then used as input for the partial autocorrelation function from the statsmodels Python package. We computed the 95% confidence interval and calculated autocorrelation across a range of lags to identify periodic trends, which were visualized using autocorrelation plots.

Thermal activity tracking

Still images were captured using the FLIR Lepton 3.5 (Teledyne FLIR, Wilsonville, OR) attached directly to a Raspberry Pi Zero 2 W computer or to a PC via a PureThermal 3 adapter (GroupGets, Reno, NV). An IR-transparent zinc selenide disk was used to construct an imaging window for the thermal camera. Images were sectioned according to the Image Processing For Mus and Hamsters section above. Cropped images were then binarized and the difference between the L2 norms of two adjacent frames was used as a proxy of activity for downstream analysis. Again for heatmap visualization, a max and min normalization value was set using 30 break histogram binning. For the cumulative activity plots, activity levels for each time point were convolved with a kernel of one hundred ones, max pooled with a block size of 100 and the daily sum was plotted as time series bar plots. These cumulative activity values were then used as input for the partial autocorrelation function from the statsmodels Python package. We computed the 95% confidence interval and calculated autocorrelation across a range of lags to identify periodic trends, which were visualized using autocorrelation plots.

Vaginal Swabbing, cytology & analysis

A cohort of 64 *Peromyscus* was monitored via camera to determine their ovulation timing. Every 6 h starting from midnight on the night of ovulation, vaginal samples were collected from groups of 4 *Peromyscus* using sterile nasopharyngeal nylon flocked swabs (SNT Biotech, Plainfield, IL) moistened with 1× sterile phosphate buffered saline (PBS). The swabs were inserted roughly 2mm into the vagina, rotated 10 times, then the sample was transferred onto individual slides (one per mouse) and left to dry. Slides were fixed

by submerging in methanol (Volu-Sol, Salt Lake City, UT) for 45 s and air-dried. Following fixation, slides were stained with the Epredia Three-Step Stain Kit (Epredia, Kalamazoo, MI). All slides were digitally captured using the TissueFAXS SL Q confocal scanner (TissueGnostics USA, Los Angeles, CA) at 10× magnification and images were saved in.tif format at 2048 × 2048 pixels with hundreds of unique images per slide/mouse. For analysis, 3 highly confluent images from each slide/mouse were selected; cells within these images were counted using the Cell Counter plugin in ImageJ software (National Institutes of Health, Bethesda, MD), and classified as cornified, leukocyte, or nucleated. The average count of each cell type across all 3 images was calculated and graphically represented against the sample collection time.

Machine learning using vaginal cytology

120 camera-tracked mice were used for this study. Equal numbers of mice representing all 4 estrous days were swabbed daily at 9a.m. until all 120 mice had been swabbed once. Samples were processed and scanned using the same reagents and procedures described in the Vaginal Swabbing section above. Images were screened for blurriness by selecting images with variance of Laplacian less than 6. Cell density of each image was estimated using an algorithm which detects the contours of particles after thresholding and computes the convex hull areas, keeping only particles with areas greater than 5. Blurry images or images with cell density less than 30 were removed from analysis. Then, images were preprocessed by rescaling to 244 × 244 × 3 followed by normalization. Data augmentation was performed by randomly flipping images horizontally. 108 mice with high quality images were randomly divided into training and validation splits at a 80%/20% ratio five times, with a model trained each time on the training set. A pre-trained ResNet-50 model was fine-tuned for 25 epochs and the best model weights, as determined by validation accuracy, were saved for prediction. Final predictions were made in an ensemble setting where softmax outputs were averaged. The remaining twelve mice unseen by the model during training and validation were then used as test data to evaluate the ensemble model's performance.

Peromyscus perfusion, tissue processing and histology

A cohort of old female mice (133–155 weeks old) were placed on camera and monitored until cycling activity could be confirmed. Three cycling and three non-cycling mice were chosen for further histological analysis. The reproductive system of mice that appeared to be cycling were collected on the day of presumed estrus.

Briefly, mice were anesthetized with isoflurane and perfused transcardially with phosphate buffered saline (PBS) as previously described.[73] Vagina/uterus were immersed fixed in 10% neutral buffered formalin, routinely processed, paraffin embedded, sectioned at 4 μm and stained with hematoxylin and eosin (H&E). Slides contained cross sections of the uterine horns and a longitudinal section of the distal uterus with adjacent conjoined cervix and vagina as per Johnson et al.[74] Ovaries were embedded in Tissue-Tek O.C.T. Compound, frozen on dry ice, and step-sectioned through the specimen at 100 μm intervals. Each resulting 6 μm section was manually H&E stained.

All slides were digitally captured using the Aperio AT2 scanner (Leica Biosystems, Buffalo Grove, IL) at 20× magnification and images were saved in.svs format.

The *Peromyscus* estrous cycle staging and evaluation of the female reproductive system for evidence of reproductive aging was performed by a board certified veterinary pathologist based on published literature for rodents.[49–51,75]

Histological analysis

To our knowledge, the histology of the estrous cycle in *Peromyscus*, as well as information on *Peromyscus* reproductive aging, has not been previously published. Therefore, our interpretation of *Peromyscus* reproductive histology is primarily based on extensive literature on rats, with additional insights from fewer studies on mice and hamsters.

Estrous cycle evaluation for each Peromyscus *in this study*

***Peromyscus* IDs: 1122, 1047 and 1118** are in estrus. Changes in the ovaries are characterized by large antral (F2) follicles, newly formed small basophilic corpora lutea (CL) and prominent eosinophilic CL with luteal cell apoptosis from previous cycles. Uterus has a tall and columnar epithelium with low number of scattered epithelial apoptotic cells and luminal dilation. Within the vagina, visible shedding of the cornified layer is present along with sloughed cornified cells and debris in the lumen.

***Peromyscus* ID: 1117** has Persistent Estrus with signs of ovarian aging characterized by many atretic follicles and lack of corpora lutea. The uterus displays early signs of endometrial hyperplasia and there is cornification of the vaginal epithelium.

***Peromyscus* ID: 1116** has Persistent Diestrus with signs of ovarian aging showing no new CL and very few older CL, and atretic follicles. The endometrial epithelium is low cuboidal and there is some areas of mucification of the vaginal epithelium.

- **Signs of ovarian aging:** The ovary contains few new follicles (approaching complete follicular depletion) and all appear atretic. There is an absence of new corpus lutea (CLs) with basophilic cytoplasm, and an overall reduced CL count.[50,76]
- **Signs of persistent diestrus in the uterus:** As with persistent diestrus in rats, the endometrial epithelium is low, cuboidal and inactive.[50]
- **Signs of persistent diestrus in the vagina:** The vaginal epithelium appears low and somewhat mucified, consistent with observations of persistent diestrus in rats.[50]

***Peromyscus* ID: 1048** is described as a mouse with an Aging Pathology characterized by a small ovary nearing anestrus with very few atretic follicles and abundant pigmented stromal tissue. The uterus has evidence of cystic endometrial hyperplasia with concurrent pyometra characterized by numerous dilated glands filled with hemorrhage, proteinaceous material and numerous degenerated neutrophils and cell debris. Numerous neutrophils were also present within the endometrial stroma. The vaginal epithelium was cornified with sloughed cornified cells and degenerated neutrophils, cell debris and hemorrhage within the lumen.

- **Signs of ovary nearing anestrus:** As observed in mice and rats, the ovary is smaller and contains few follicles, with near-complete follicular depletion. All follicles are atretic, precluding ovulation. Furthermore, an absence of corpus lutea and an increase in stromal tissue with prominent pigment in the interstitium are noted, indicative of aging in mice and rats.[50,76] Notably, this mouse presents with pyometra. However, pyometra/inflammation is not believed to be the cause of ovarian atrophy. Pyometra is an inflammatory condition of the uterus that may arise when the normal flora becomes opportunistic under certain conditions. The observed ovarian atrophy likely results from ovarian exhaustion due to hormonal dysregulation associated with aging.
- **Signs of aging in the uterus:** Reproductive tract pathology confirms the mouse's non-cycling status, with histologic evidence of cystic endometrial hyperplasia and pyometra. In aging mice and rats, CEH disrupts the estrus cycle and can lead to a phenotype of persistent estrus through hormonal dysregulation (Dixon, 2014). Pyometra can be an infection overlying CEH and is reported in dog.[77]
- **Signs of aging in the vagina:** The morphological features of the vagina provide evidence of hormonal dysregulation or persistent estrus, characterized by a visibly shedding cornified layer. Additionally, the presence of numerous degenerated neutrophils and red blood cells in the lumen indicates inflammation.

Homology arm sequences for targeting constructs

5′ Rosa26 homology arm

GGTGGTCAGGGCCATGGTCCGCCCTGCCGCAACCGGAGGGGGTGGGAGGAGGGAGCGGAAAGATCTCCACCGGACGCGGCC
ATGGCTCCCACGGGGGGCGGAGGAGCGCTTCCGGTTCCCGTCTCGTCGCTGATTGGCCTTTTCTCCTCCCGCCGTGTGTAAAAA
CACAAATGGCGTGTTTTGGTTGGAGTGAAGCGCCTGTCAGTTAACGGGTGCTGGAGTGCGCAGCCGCTGGCTGCCTCGCTGTGCC
CACTGGGTGGGGCGGGAGGTAGGTGGGGTGAGGAGAGCTGGACGTGCGGGCGCGGCCGGCCCCTGGCGGGGCGGGGGAAGG
GAGGGGAGGGAGGGTCAGCGAAAGTGGCTGGCGCCCAGGCGGCCTCCCACCCTCCCCTTCCTCTGGGGGAGTCGGTTTACCCG
CCGCCGGCCTGGCCTCGTCGTCTGATTGGCTCCCGGGGCCCAGAAAACTGGCCCCTGCAATTGGCCCGCGTTCGTGCAAGTTCAG
TCCATACGCGGGCTGGCGGGGGCGGCAGGGAGGCGCTCGCAGGTTCCGGCCCTCCCCAAGGCCCCGCGCCGCAGAGTCTGG
CCCCGCGCCCCTGCGCAACGTGGCAGGAAGCGCGCGCTGGGGGCGGGGACGGGCAGGCGGTCTGAGCGGCGGGGCGGGGG
CGAGCGCGGTTCCTCCTAGAGTTGTTGCCGCACGAGGGGCGAGCTGAACCGGACCTGCATGGCGCACTCCTAGGAGTGGAG
GAAGGAGTGGGGGCTCAGTCGGGCCGGTTTGGAGGCAGGAGGCACTTGCTCTCCAAAATTCCGTGAGAGCTGCAATCAATAA
GGGAGCCGCAGTGGAGTAGGCGGGGAGAAGGCCGCACCCTTCTCGGCAGGGGGAGGGGAGTGCCGCAATACCTTTCTGGG
AGTTCTCTGCTGCCTCCTGGCTTCTAAAGACCGCCCCGGGCCTGGAACAGTCCCTTCCCCCTCTCCCCTCGTGATCTGCAAGTCG
AGGCTTTCTGGA

3′ Rosa26 homology arm

AGATGGGCGGGAGTCTTCTAGGCTGGCTTAAGGGCTAACCTGGTGCGTGGGCGTTGTCCTGCAGGGGAATTGAACAGGTTTAAA
ATTGGAGAAACGACACTTCCCACAGATTTTCGTTTGTGTCCGGAGGGAATTGTAATAGGAGCAAAGGAGGGAAATGGGTGACT
AGGCGCTCACCTGGGGTTTTATGCAGCAAAACTACAGGTTATTATTGCTTATGATCTGCCTTGAAGTATTTTTCATCGTGTTAGA
TTAAAGACATGCTCACCCAAGTTTATACTCCCACTTGAGATCCTTGTTATATCATGAAATTTTAGTATCGTAAATTAGAATATATAA
ACAGAATCTTAGCAGTTTCTGCAGAGCCCAGTGCTTCACTCTGTCCCTCTTGCTCCCTCTGCAGCCCTACCAAGAGATATTTTA
GCGCTCTCTCATTTTAGTCCCGTTTTCATTTGTTGTACTGGCTTATCCAATCCCTAGACAGAGCACTGGCATTCTTCCTCTCCTA
TCTTAGAAGCCTGATGAGTCATGAAACCAGACAGATTAGTTACACCACAAATTGAGGCTGTAGCTAGGGCCTTGCCCTGCAGT
TCTTTTATTCCTCCTTAGTACATTTTGTTGACTGTTTGCCTTGATTTCATTTTCTATCCCCACCCTTCAGGAGCTTTACTACAATA
GATTTATTGAGAATCTAACCTAAAGTTCAGCTTCTTTCCACTCCCATGTATGCCTATCTCCTTTTTCACCATTAATAAACTGAACT
GTTATTAATGGCTTCCAGATGGATGTCTCCTCCAATATCACCTGATGTATCTTACATATCGTCAGGCTGATTGTATTAAAAGGTA
CATGAATTGACATGAAATTTACTGACTCCTTAATGCTTTAGTGGATTCCATGAGTACAATACAGAAGACCGTTAATGGGCTACT
GACAGCTTTTTCATTTCATTATTTCCTGCATACACACTTTGAGTCACATGGAATTGATTACTGCTTA

QUANTIFICATION AND STATISTICAL ANALYSIS

Quantitative analyses were performed using the sample sizes and biological replicates described in the figure legends and STAR Methods. Summary statistics and measures of variability are reported as indicated. Statistical comparisons for biological experiments were limited to tests of proportions or other categorical outcomes, and the corresponding figure legends specify all tests, significance thresholds, and any adjustments for multiple comparisons. Machine-learning models used for estrous-stage classification were trained and evaluated as described in the STAR Methods, including details on training/validation splits, performance metrics, and cross-validation procedures. No additional statistical modeling beyond these analyses was applied.